

Spurious Features Everywhere - Large-Scale Detection of Harmful Spurious Features in ImageNet

Yannic Neuhaus, Maximilian Augustin, Valentyn Boreiko, and Matthias Hein

University of Tübingen

Abstract

Benchmark performance of deep learning classifiers alone is not a reliable predictor for the performance of a deployed model. In particular, if the image classifier has picked up spurious features in the training data, its predictions can fail in unexpected ways. In this paper, we develop a framework that allows us to systematically identify spurious features in large datasets like ImageNet. It is based on our neural PCA components and their visualization. Previous work on spurious features of image classifiers often operates in toy settings or requires costly pixel-wise annotations. In contrast, we validate our results by checking that presence of the harmful spurious feature of a class is sufficient to trigger the prediction of that class. We introduce a novel dataset “Spurious ImageNet” and check how much existing classifiers rely on spurious features.¹

1. Introduction

Deep learning has led to tremendous progress in several application areas such as image classification [29, 36] or natural language processing [13]. Over the years, however, it has become apparent, that evaluating predictive performance on a fixed test set is not necessarily indicative of the performance when image classifiers are deployed in the wild. In fact, several potential failure cases have been discovered. This starts with a lack of robustness due to image corruptions [24], adversarial perturbations [52], and arbitrary predictions on out-of-distribution inputs [23, 25, 34]. In this paper, we consider the problem of spurious features to debug image classifiers [2]. Spurious features in image classification are features that co-occur with the actual class object and are picked up by the classifier. In the worst case, they lead to shortcut learning [20], where only the spurious but not the correct feature is associated with the class, e.g., [60] found that a pneumonia detector’s bad generalization across hospitals was because the neural network had



Figure 1. **Top:** Examples of spurious features found via our neural PCA components but not in previous study [45]. **Bottom:** We validate our spurious features by mining images from the web showing **only the spurious feature but not the class**. They are classified by four ImageNet models as the corresponding class. Some contain even ImageNet classes (bees on feeder, grasshopper in leaves).

learned to identify the hospital where the training data was coming from. A weaker form of spurious feature (at least from a learning perspective) is the case when the classifier picks up the correct class features, e.g., of a hummingbird, but additionally associates a spurious feature, e.g., a bird feeder, with the class as they appear together on a subset of the training set. This becomes a harmful spurious feature if *only* the spurious feature *without* the class feature is sufficient to trigger the classification of that class, see Fig. 1 for an illustration of such spurious features found via our method. Such harmful spurious features are more difficult to detect, and thus can easily go unnoticed leading to unexpected behaviour of a deployed image classifier.

¹https://github.com/YanNeu/spurious_imagenet.

In this paper we make the following key contributions:

- we develop a pipeline for the detection of spurious features with little human supervision based on our class-wise neural PCA components of an adversarially robust classifier together with their Neural PCA Feature Visualization (NPFV). Our neural PCA components have a direct interpretation in terms of class logits.
- in contrast to prior work, we validate our found spurious features not by masking the class object or spurious features which requires pixel-wise annotations. Instead, we use the neural PCA component together with minimal human supervision to find images containing the spurious feature but not the class object.
- using these images we create the “Spurious ImageNet” dataset and propose a measure for dependence on spurious features. We do a large-scale evaluation of state-of-the-art (SOTA) ImageNet models. We show that the spurious features found for the robust model generalize to non-robust classifiers. Moreover, we examine how pre-training on ImageNet21k affects spurious dependence.
- we show that for the model that has been used to compute neural PCA components, strong mitigation of the dependence on spurious features is possible without requiring re-training or fine-tuning.

2. Related work

When classifiers in safety-critical systems such as healthcare or autonomous driving are deployed in the wild [3], it is important to discover potential failure cases before release. Prior work has focused on corruption [24], adversarial robustness [10, 32, 52], and out-of-distribution detection [23, 25, 34]. There is less work on spurious features, although their potential harm might be higher.

Spurious features: It has been noted early on that classifiers show reliance on spurious features [14] e.g., a cow on the beach is not recognized [8] due to the missing spurious feature of grass. Other forms of spurious features have been reported in the classification of skin lesions [11], pneumonia [60], traffic signs [51], and object recognition [61]. Moreover, it has been shown that deep neural networks are biased towards texture [21] and background context [59], see [20] for an overview. [42] argues theoretically that spurious features are picked up due to a simplicity bias.

Detection of spurious features has been achieved using human label-intense pixel-wise annotations [35, 43, 44]. In [58], they use sparsity regularization to enforce a more interpretable model and find in this way spurious features. In [4], they propose a complex pipeline to detect spurious features. While they scale to ImageNet, their analysis is limited to a few spurious features for a subset of 100 classes. A search for full ImageNet is done in [33, 45, 46] based on class-weighted “neural maps”. The neural maps are used to add noise to “spurious” resp. “core” features but no signif-

icant difference in classification performance is observed. Thus, while human labelers have marked features as spurious it remains unclear if these features are powerful enough to force the class decision on images only showing the spurious feature and not the class.

Interpretability methods: In recent years several interpretability methods, some of them targeted particularly towards deep learning classifiers, have been proposed e.g., attribution methods such as GradCAM [41], Shapley values [31], Relevance Propagation [7], and LIME [37]. The use of these methods for the detection of spurious features has been analyzed in [1, 2] with mixed success and it has been argued that interpretability methods are not robust [17, 22, 48]. However, [19] note that attribution methods work better for robust classifiers due to more interpretable gradients. Another technique is counterfactual explanations [56, 57]. Their generation is particularly difficult for the image domain due to the similarity to adversarial examples [52]. Thus visual counterfactual explanations have been realized via manipulation of a latent space [40] or directly in image space [6, 12, 39] for an adversarially robust classifier even for ImageNet. Visual counterfactuals for non-robust classifiers have been developed in [5] using diffusion models [16, 26, 28, 49, 50].

ImageNet: ImageNet [38] suffers from several shortcomings: apart from an inherent dataset bias [53], semantically overlapping or even identical class pairs were reported [9, 27, 54], e.g., two classes “maillot”, “sunglass” vs “sunglasses”, “notebook” vs “laptop” etc. We disregard such trivial cases of dataset contamination and focus on classes with harmful spurious features, in particular, those that arise when only a small portion of the training set is contaminated with a spurious feature.

3. Spurious features

A proper definition of spurious features is difficult. We discuss the two main types which appear in this paper. A *correlated feature* is a feature that occurs frequently with the class object in the training set (bird feeder as correlated feature of class “hummingbird”) but there is no causal implication that appearance of the class object implies appearance of the spurious feature (appearance of hummingbird does not imply presence of a bird feeder). A *correlated feature* becomes a *spurious feature* when the classifier picks it up as feature of this class. Not every spurious feature is immediately harmful, even humans use context information [20] to get more confident in a decision. However, a spurious feature is *harmful* if the spurious feature alone is enough to trigger the decision for the corresponding class without the class object being present on the image.

We fix notation and describe two harmful settings of spurious features. Let $\mathcal{D} = (X_i, Y_i)_{i=1}^N$ be a (training) dataset for supervised classification where each X_i is an image be-

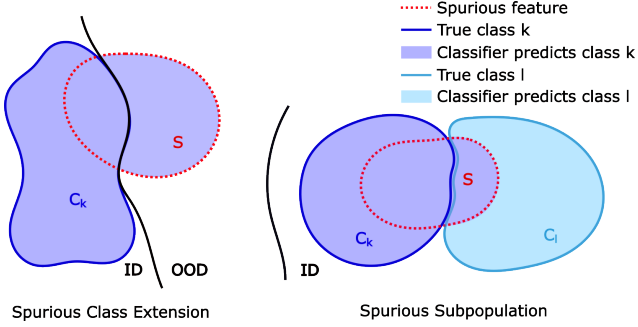


Figure 2. **Type of Spurious Feature:** Left: The spurious feature S appears in in- and out-of-distribution and the classifier extends the class from C_k to $C_k \cup S$. Right: The spurious feature is shared between classes but appears more often in one class. Hence, the classifier learns to associate class $C_l \cap S$ with class C_k .

longing to the set of classes, $Y_i \in \{1, \dots, K\}$. On the population level, we denote by \mathcal{A} the set of all images and $C_k \subset \mathcal{A}$ is the set of all images containing objects belonging to one class k (assuming for simplicity that we have a deterministic problem and ignoring multi-labels).

A *correlated class or feature* S for class C_k is a set of images where $C_k \cap S$ and $S \setminus C_k$ are non-empty. Note that a specific S can be a correlated feature for several classes e.g., a certain background like trees for pictures of apes. A correlated feature becomes *spurious* when it is picked up by the classifier. In this paper, we consider two main scenarios for a *harmful spurious feature* shown in Fig. 2.

Spurious Class Extension: In this type of spurious feature (left in Fig. 2) the classifier picks up the spurious feature S for class k and predicts even on $S \setminus C_k$ the class k with high confidence (prediction of “hummingbird” for images showing a bird feeder but no hummingbird). Thus the classifier predicts class k beyond its actual domain C_k and thus we call this spurious class extension. While this spurious feature does not necessarily hurt in terms of test performance it can easily lead to completely unexpected behavior when the classifier is deployed in the wild.

Spurious Subpopulation: Here, two classes C_k and C_l share a spurious feature S (e.g., “water jet” for the classes “fireboat” and “fountain”). As there are more training images with feature S in C_k than in C_l the classifier predicts images of class C_l as class C_k .

Note that this is not an exclusive property, and there can be spurious class extensions and spurious subpopulations for a feature S at the same time. In the experiments, we will see both cases, e.g., the object bird feeder leads to a spurious class extension of the class “hummingbird” (see Fig. 4) to images of bird feeders **without** hummingbirds. Almost all training images containing this feature belong to this class. Therefore, as shown in Fig. 4 top row right, test images of bees on a bird feeder are still classified as “hummingbird”

instead of “bee” (spurious subpopulation).

In the next section, we define our pipeline to identify spurious features in the training set of ImageNet with minimal human supervision.

4. Finding spurious features via neural PCA and associated feature visualizations

In prior work, it has been observed [6, 12, 39, 45, 55] that adversarially robust models have generative properties in the sense that maximizing the predicted probability of a certain class in a neighborhood of an initial image leads to semantically meaningful changes. Moreover, adversarially robust models have more informative gradients [19] and thus attribution maps such as GradCAM [41] work better. Thus, we use an adversarially robust model, similar to [45], to find spurious features in ImageNet. In particular, we use the multiple-norm robust model from [12] which they report to have the best generative properties. We validate all our findings by showing that non-robust ImageNet models share the same spurious features (Fig. 4 and Sec. 6.2).

First, we define our class-wise neural PCA which allows us to find subtle spurious features due to small subpopulations in the training data of a class, e.g., we checked that the bird feeder object for “hummingbird” is clearly visible in 15% of the training images (component 2), while another 15% contain just a small part of it (component 3), see Fig. 3 or, for more examples, App. C. Then we discuss our neural PCA feature visualization and the selection procedure of the considered components for inspection. The final identification of spurious features requires human supervision, and we describe an effective setup that allows us to screen all ImageNet classes for spurious features.

4.1. Class-wise neural PCA and its interpretation in terms of class logit

We consider the features of the penultimate layer $\phi(x) \in \mathbb{R}^D$ of a given neural network and input x . For a given class $k \in \{1, \dots, K\}$ and its associated weights $w_k \in \mathbb{R}^D$ in the final layer, we define, \odot being componentwise product,

$$\psi_k(x) = w_k \odot \phi(x). \quad (1)$$

Let $b \in \mathbb{R}^K$ be the bias vector of the final layer then the logit f_k of class k can be written as

$$f_k(x) = \langle \mathbf{1}, \psi_k(x) \rangle + b_k = \sum_{j=1}^D w_{kj} \phi(x)_j + b_k \quad (2)$$

Let J_k be the set of all training images classified as class k . In [45], they consider the class-wise mean over predictions,

$$m^{(k)} = \frac{1}{|J_k|} \sum_{x_s \in J_k} \psi_k(x_s), \quad (3)$$

and denote the j -th component $m_j^{(k)}$ as the importance of the j -th neural feature for class k . They considered the top

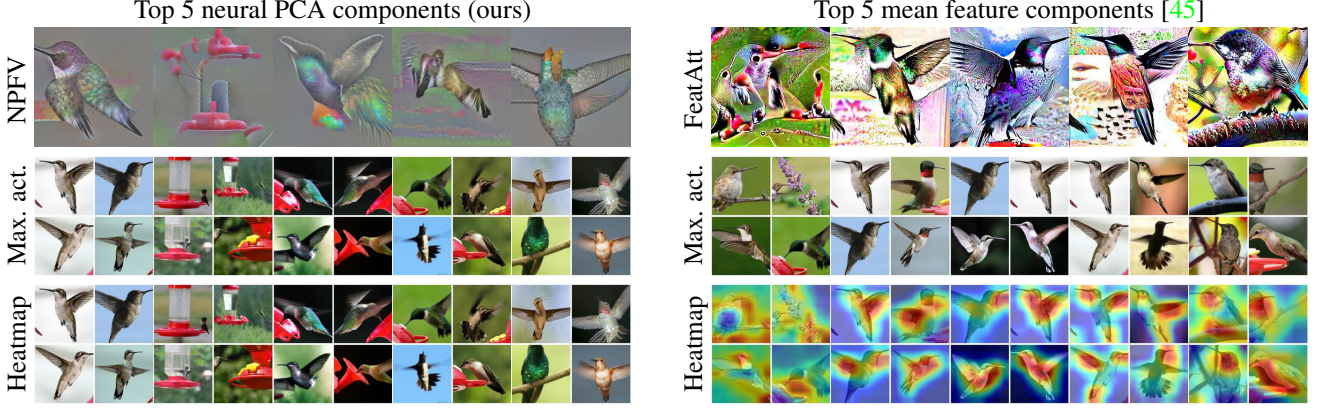


Figure 3. **Neural PCA feature components vs neural features of [45] for class hummingbird**: The first row shows our neural PCA feature visualization (NPFV) of our top 5 neural PCA components (left), and the feature attacks of the top 5 neurons of [45] (right). The second row shows the four most activating training images of the components/neurons and the last row GradCAM for the neural PCA components (left) and the neural activation map of [45] (right). Our neural PCA components are capturing different subpopulations in the training data. Component 2 is identified as spurious feature “bird feeder”, see NPFV and most activating training images (see also Fig. 4). The top 5 neural features of [45] do not show the spurious feature “bird feeder” as they are based on mean activations over the training set, and thus not sensitive enough to small subpopulations. Note that their neurons 2,3, and 4 are very similar (overlap in most activating images) and don’t capture the variety of the training set. Their first component has been labeled as spurious background.

five neural features and visualized them in form of a “neural activation map”. While this approach can identify strong spurious components, it has the disadvantage that it is not very sensitive, see Fig. 3 and Sec. 6.2. Looking only at the mean on the training set, it is very difficult to detect spurious features picked up by the classifier due to contamination of a small portion of the training set.

Let I_k be the index set of training instances of class k and let $\bar{\psi}_k$ be the class-wise mean, $\bar{\psi}_k = \frac{1}{|I_k|} \sum_{s \in I_k} \psi_k(x_s)$. We consider in this paper the *class-wise neural PCA* which allows to pick up variations in the set $(\psi(x_r)_{r \in I_k})$ arising due to small subpopulations in the training set. In the class-wise neural PCA we compute the eigenvectors of the class-wise covariance matrix,

$$C = \sum_{s \in I_k} (\psi_k(x_s) - \bar{\psi}_k)(\psi_k(x_s) - \bar{\psi}_k)^T, \quad (4)$$

which we denote by v_1, \dots, v_D . They form an orthonormal basis of \mathbb{R}^D and we develop $\psi_k(x) - \bar{\psi}_k$ into this basis,

$$\psi_k(x) - \bar{\psi}_k = \sum_{l=1}^D v_l \langle \psi_k(x) - \bar{\psi}_k, v_l \rangle, \quad (5)$$

and define

$$\alpha_l^{(k)}(x) = \langle \mathbf{1}, v_l \rangle \langle \psi_k(x) - \bar{\psi}_k, v_l \rangle, \quad (6)$$

The logit $f_k(x)$ of the k -th class can then be written as

$$f_k(x) = \sum_{l=1}^D \alpha_l^{(k)}(x) + \langle \mathbf{1}, \bar{\psi}_k \rangle + b_k. \quad (7)$$

Thus for a given input x , we can interpret $\alpha_l^{(k)}(x)$ as the contribution of the neural PCA component l of class k to

the logit $f_k(x)$ of class k since the term $\langle \mathbf{1}, \bar{\psi}_k \rangle + b_k$ is constant for all inputs. A fix of spurious neural PCA components without re-training based on this is discussed in Sec. 5. In Fig. 3, we illustrate that our top selected neural PCA components can identify small subpopulations in the training data which is not feasible for the neural features of [45].

4.2. Neural PCA Feature Visualization

To identify the semantic features corresponding to our neural PCA component $\alpha_l^{(k)}(x)$, we show the training images with the largest values. Additionally, we generate an image by maximizing $\alpha_l^{(k)}(x)$. More specifically we consider the optimization problem,

$$z_l^{(k)} = \operatorname{argmax}_{\|g\|_2 \leq \epsilon} \alpha_l^{(k)}(g + \delta),$$

where g is an image with gray pixels (all channels equal to $\frac{1}{2}$). Thus maximizing the feature $\alpha_l^{(k)}$ outgoing from a non-informative and unbiased initialization g . The optimization problem is solved using adaptive projected gradient descent (APGD) [15] with 200 steps. The budget for changes is small ($\epsilon = 30$) to avoid the overactivation one sees in the feature attacks where the output of individual neurons is maximized [18, 45, 47], see Fig. 3. We call the image $z_l^{(k)}$, maximizing the feature, the **Neural PCA Feature Visualization (NPFV)** of feature l of class k . In Fig. 4 we show for each identified spurious feature component, the corresponding NPFV. For each class, the NPFV mainly shows the spurious feature and no, or only to a small extent, class-specific features, e.g., for “hummingbird” one can clearly see the bird feeder but not a hummingbird.

4.3. Selection of neural PCA components for human inspection

The penultimate layer of the robust network ResNet50 we are using has 2048 neurons. Thus it would be absolutely infeasible (and also unnecessary) to investigate all the neural PCA components. A strong criterion that one has found a harmful spurious feature is: i) the NPFV shows mainly the spurious feature and not the class, ii) the NPFV has high confidence. If ii) is not fulfilled, then the NPFV is still a spurious feature the classifier has potentially picked up but it is not harmful in the sense that this feature alone can trigger the classifier to decide for this class. Moreover, we noticed that the eigenvalues of the neural PCA as well as the corresponding α values decay quickly. Thus we compute the NPFV for the top 128 neural PCA components (having maximal variance) and then select the ten components which realize the highest confidence for their NPFV in the corresponding class. Note that we do not optimize the confidence when generating the NPFV but only $\alpha_l^{(k)}$ which is part of the logit of the k -th class.

4.4. Identification of spurious neural PCA components via human supervision

For each ImageNet class k we show the human labeler the top 10 components. For each component l we show the NPFV $z_l^{(k)}$ and the 5 training images x_r of class k with the largest values of $\alpha_l^{(k)}(x_r)$. Moreover, we compute GradCAM [41] images for the NPFV and the five training images using the neural PCA component $\alpha_l^{(k)}$ as score. The human marks a component as spurious if i) the NPFV shows dominantly an object not belonging to the class or background features, ii) the five training images show consistently this object or background, iii) the GradCAM images show activations dominantly not on the class object. The setup shown to the human labeler can be seen in App. B. The labeling of one class takes on average about 45 seconds so the full labeling of all ImageNet classes took about 13 hours. The human labeler (researcher in machine learning) found in total 337 spurious components. Another human labeler went through the total list, removing the spurious feature in case of disagreement, resulting in 319 components of spurious features from 230 ImageNet classes. While our spurious features and the ones of [45] are not necessarily similar for the same class, see Fig. 3 for “hummingbird”, we want to give a rough idea of how the found features relate. In total [45, 46] report 630 spurious features in 357 classes. The overlap of classes where both methods find spurious features is 129, whereas there are 101 classes where only we find a spurious feature and 228 classes where only they report one. While a full validation of all our found spurious features is out of reach we validate a subset of 40 spurious features in our novel “Spurious ImageNet” dataset in Sec.

6.2 including 11 which only we found, see Fig. 1.

5. Mitigation of spurious features

Once the spurious features are identified, the question is how one can mitigate that the classifier relies on them. One way is to identify the training images containing the spurious feature and then discard or downweight them during training. However, this would require relabeling all spurious ImageNet classes which is not feasible. Using the corresponding neural PCA component $\alpha_l^{(k)}$ we could order the training set according to this value which indicates how much of the spurious feature it contains. While this would speed up the process significantly, it would still require a significant amount of manual relabeling. Can one do it also without any additional labeling? Yes, as described in Sec. 4 we can rewrite the logit of the k -th class as

$$f_k(x) = \sum_{l=1}^D \alpha_l^{(k)}(x) + \langle \mathbf{1}, \bar{\psi}_k \rangle + b_k. \quad (8)$$

For an identified a spurious component l of class k , we use instead of $\alpha_l^{(k)}$ the value $\min\{\alpha_l^{(k)}, 0\}$ to take this feature out of the logit. This significantly reduces the effect of spurious features, see Sec. 6.3.

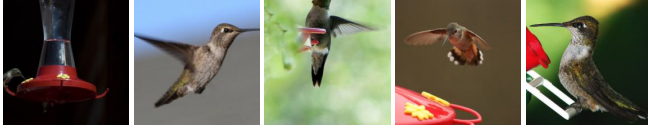
6. Experiments

In this section, we provide a qualitative and quantitative evaluation of our 319 detected spurious features in ImageNet, see Sec. 4.4. For the quantitative evaluation, we create the dataset “Spurious ImageNet”, which allows checking the reliance of a given ImageNet classifier on spurious features. We also evaluate our mitigation strategy which does not require any retraining of the classifier.

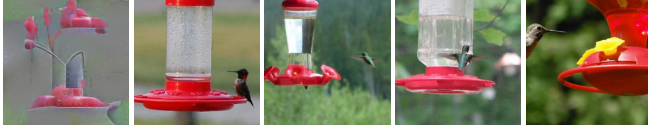
6.1. Qualitative evaluation:

For the qualitative evaluation, we visualize some of our found 319 spurious features, see Fig. 4. For each class, we show five random training images, the NPFV, and the four most activating training images of the neural PCA component labeled to be spurious. Additionally, we show always ten images which **only** show the spurious feature but **not** the actual class e.g., only the bird feeder (spurious) but no hummingbird (class). All ten images are classified as the corresponding class for the robust classifier we have used to compute the neural PCA components and three non-robust ImageNet classifiers (ResNext101, Eff.Net B5, ConvNext-Base) which have been trained on ImageNet, (first four entries in Tab. 1). This shows that our spurious features generalize from the robust classifier to SOTA ImageNet classifiers, indicating that the found spurious features are mainly due to the design of the training set, rather than failures in model training. Our novel validation by showing examples of images with the spurious feature but without the class

Hummingbird - Random train. images (**confidence** / α_k)

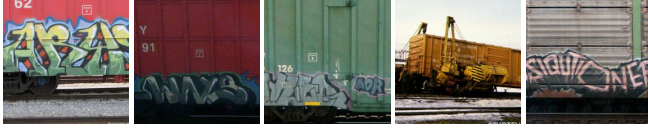


0.93/1.7 1.00/-0.9 0.96/-1.0 0.99/2.2 1.00/1.54
NPFV-2 Max. activating train. images - N-PCA Comp. 2

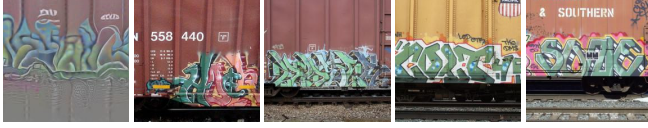


1.00/9.7 1.00/7.5 1.00/5.9 1.00/5.6 1.00/5.6

Freight car - Random train. images (**confidence** / α_k)

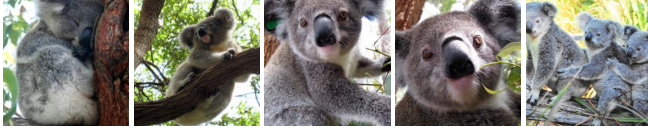


1.00/7.7 1.00/3.4 1.00/6.3 0.98/-0.8 1.00/4.2
NPFV-1 Max. activating train. images - N-PCA Comp. 1



1.00/12.1 1.00/10.9 1.00/10.4 1.00/10.2 1.00/10.2

Koala - Random train. images (**confidence** / α_k)

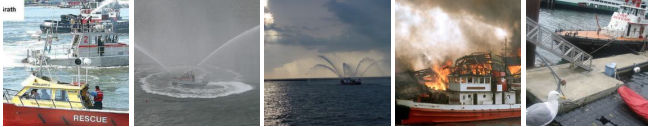


1.00/0.77 0.87/2.4 1.00/0.4 1.00/0.0 0.95/0.5
NPFV-3 Max. activating train. images - N-PCA Comp. 3



1.00/5.5 1.00/4.6 1.00/4.5 1.00/4.4 0.86/4.3

Fireboat - Random train. images (**confidence** / α_k)

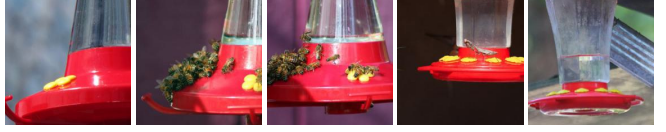


0.88/-1.1 0.95/0.5 0.12/-0.6 0.84/-0.2 0.02/-1.1
NPFV-2 Max. activating train. images - N-PCA Comp. 2

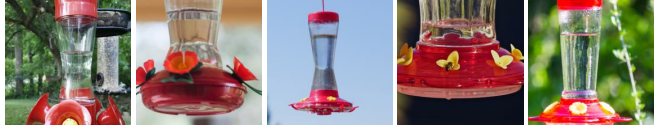


1.00/5.5 0.42/4.1 1.00/4.0 1.00/3.9 1.00/3.9

Images with spurious **bird feeder** but **no hummingbird**



0.94/5.7 0.94/3.4 0.82/2.9 0.91/5.6 0.91/4.7
all classified as **humming bird** by four ImageNet models

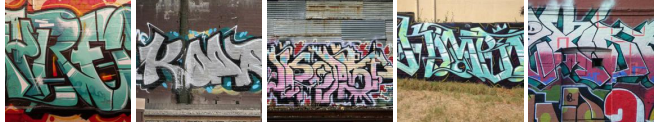


0.86/4.3 0.81/3.5 0.89/3.3 0.89/3.8 0.78/5.91

Images with spurious **graffiti** but **no freight car**



0.97/3.5 0.79/4.0 0.81/2.4 0.85/3.2 0.88/2.6
all classified as **freight car** by four ImageNet models



0.85/2.5 0.86/2.5 0.90/2.3 0.82/2.2 0.87/2.2

Images with spurious **eucalyptus/plants** but **no koala**



0.49/3.5 0.61/3.1 0.36/3.1 0.36/3.1 0.69/2.7
all classified as **koala** by four ImageNet models



0.56/2.6 0.62/2.5 0.74/2.5 0.72/2.4 0.66/2.2

Images with spurious **water jet** but **no fireboat**



0.63/2.3 0.71/2.2 0.84/2.2 0.65/2.1 0.63/1.9
all classified as **fireboat** by four ImageNet models



0.53/1.9 0.79/1.9 0.78/1.8 0.79/1.8 0.76/1.8

Figure 4. **Spurious features (ImageNet):** found by human labeling of our neural PCA components. For each class we show 5 random train. images (top left), the neural PCA Feature Visual. (NPFV) and 4 most activating train. images for the spurious feature component (bottom left). Right: four ImageNet models classify images **showing only the spurious feature but no class object** as this class.

which are consistently classified as this class is a direct way to show the impact of harmful spurious features.

The images showing only the spurious feature were obtained by sorting the approximately 9 million images of OpenImages [30] by their values of the neural PCA component $\alpha_l^{(k)}(x)$. Then we are checking the top 625 retrieved images classified by the robust classifier as the corresponding class if they are all classified as the corresponding class by the additional non-robust classifiers *and* do not show the corresponding class. Note that this is a quite strict criterion as spurious features can be shared across classes, e.g., twigs for birds, and thus agreement of classifiers is not granted and the images can show the spurious feature *and* the true class. Nevertheless, this procedure yields between 77 (“hummingbird”) and 179 (“freight car”) examples of which we show a selection. For “hummingbird”, a lot of these images show red flowers (without a hummingbird) which makes sense as the NPFV displays features of red flowers and due to the bias that OpenImages does not contain many images of hummingbird feeders. In these cases, we additionally use Flickr images obtained with appropriate text queries e.g., “hummingbird feeder” and filter them.

We note that in the case of “hummingbird”, “freight car”, and “koala” the spurious features have significantly extended the class beyond the actual class (see Fig. 2). Bird feeders are classified as hummingbirds, graffiti as freight cars, and (eucalyptus) plants as koalas. This class extension cannot be detected by monitoring test performance, and thus is likely to be noticed only after deployment. For “hummingbird”, we see in Fig. 4 two images with bees on the bird feeder where “bee” is an ImageNet class (also a grasshopper for “koala”). Nevertheless, the spurious “bird feeder” feature of “hummingbird” is strong enough to overrule “bee” even though no hummingbird is present.

The spurious feature “water jet” is shared among the two classes: “fireboat” and “fountain”. It forms a spurious subpopulation, which appears more frequently for “fireboat” (see Fig. 2). This leads to an in-distribution shift where now a large number of images of the “fountain”-class with a water jet are wrongly classified as “fireboat”. The spurious feature “water jet” for “fireboat” has been found as well in the Salient ImageNet dataset [45, 46]. However, they did not find spurious features for freight car (the graffiti is labeled as “core feature”) and koala (in App. A we show that they don’t find this feature). They found a different spurious feature for “hummingbird”, but not the “bird feeder” (our component 2 vs their component 1 in Fig. 3). More examples are in App. C.

6.2. The Spurious ImageNet dataset

A key contribution of this paper is our novel evaluation of spurious features for image classifiers without requiring pixel-wise annotations [35, 43] or having to rely on the va-

Model	TrainSet	ImageNet Acc. \uparrow	Spurious mAUC \uparrow
Rob. ResNet50	1K	57.4%	0.629
ResNext101	1k	79.3%	0.802
EfficientNet B5	1k	83.8%	0.836
ConvNext-B	1k	83.8%	0.791
Rob. ResNet50 (SpuFix.)	1k	56.8%	0.781
Rob. ResNet50 [45]	1k	57.9%	0.645
EfficientNetv2-L	1k	85.5%	0.847
ConvNext-L	1k	84.3%	0.792
EfficientNetv2-L	1k-FT21k	86.3%	0.886
ConvNext-L	1k-FT21k	86.6%	0.900
ViT-B	1k-FT21k	84.5%	0.899
EfficientNetv2-L	21k	-	0.921
ViT-B	21k	-	0.923

Table 1. **Quantitative Evaluation on Spurious ImageNet:** we show that all ImageNet classifiers with different training modalities depend on spurious features in varying strength. The spurious mAUC is the mean of AUCs for the separation of images containing only the spurious feature but not class k versus test images of class k according to the predicted probability for class k . A spurious mAUC of 1.0 indicates no dependence on spurious features.

lidity of neural heatmaps [45]. Instead, we use images from OpenImages to show that images only containing the spurious feature but not the class object are classified as this class. This has the advantage that we consider real images and thus provides a realistic impression of the performance of ImageNet classifiers in the wild. Adding noise [45] or masking [33, 35] image regions requires pixel-wise accurate annotations which are labor-expensive, masking only the object still contains shape information, and using masks avoiding this, e.g., a bounding box around the object, can hide a significant portion of the image which is unrealistic.

In order to allow for a more quantitative analysis of the influence of spurious features on ImageNet classifiers, we collected images similar to the ones shown to illustrate the spurious features in Fig. 4. The images are chosen such that they show the spurious feature but not the class object. The only difference is that we relax the classification condition and only require two of the four classifiers (robust ResNet50, ResNext101, EfficientNet-B5, ConvNext-Base, see Tab. 1) to predict the corresponding class. We select 40 of our spurious features and for each one collect 75 images from the top-ranked images in OpenImages according to the value of $\alpha_l^{(k)}$ for which two human labelers agree that they contain the spurious feature but not class k and two out of four classifiers predict class k . We call this dataset **Spurious ImageNet** as it allows us to check the influence of spurious features on real images on ImageNet classifiers. We demonstrate samples from the dataset in App. D.

A classifier f not relying on the spurious feature should

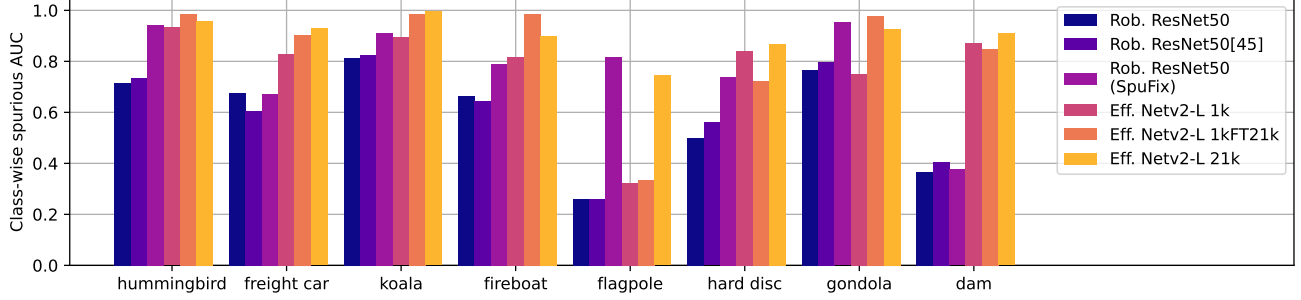


Figure 5. **Spurious ImageNet**: for 8 out of the 40 classes in the dataset we plot the AUC of different models. The classes (spurious feature) are: hummingbird (bird feeder), freight car (graffiti), koala (plants), flagpole (US flag), hard disc (label), gondola (house/river), and dam (waterfall). The robust ResNet50 of [45] performs similarly to our robust ResNet50. Thus the spurious features bird feeder, graffiti, eucalyptus, and label which have not been detected in [45, 46] are also spurious features for their model. Our mitigation SpuFix for our robust ResNet improves the AUCs significantly. Fine-tuning from 21k helps to be less dependent on spurious features and is similar in performance to native ImageNet21k classifiers. While dependence on some spurious features is almost eliminated for the EffNetv2-21k, for fireboat, hard disc, and particularly flagpole there is still a strong dependence.

predict a low probability for class k for the Spurious ImageNet samples, especially compared to test set images of ImageNet for class k . Thus, for each class, we measure the AUC (area under the curve) for the separation of images with the spurious features but not showing class k versus test set images of class k according to the predicted probability for class k . A classifier not depending on the spurious feature should easily attain a perfect AUC of 1. We compute the mean AUC over all 40 classes and report them in Tab. 1. A mean AUC significantly below 1 shows strong reliance on spurious features. We observe that all ImageNet models trained on 1k ImageNet only are heavily influenced by spurious features. This shows that the spurious features are mainly a problem of the training set and less of the classifier and that spurious features are found using an adversarially robust model transfer to standard ImageNet classifiers.

We note some of the found spurious features such as flag (flag pole), bird feeder (hummingbird), and eucalyptus (koala) have their own classes in ImageNet21k. Thus they should no longer be spurious for the other classes. Therefore we test if ImageNet 1k-classifiers fine-tuned from a ImageNet21k model are less reliant on spurious features. The results in Tab. 1 and Fig. 5 suggest that the influence of spurious features is damped but they are far from being free of them. To check how much is lost due to fine-tuning we evaluate a ViT-B trained on ImageNet21k. While for the ViT-B on ImageNet21k the mean AUC is 0.923, one of the fine-tuned model drops only slightly to 0.899 which shows that fine-tuning does not hurt much. While the mean AUC improves, a large number of classes are still not working well, showing that the spurious feature has not been resolved. Surprisingly, this is true even for classes like freight car, where the spurious feature “graffiti” is its own class in ImageNet21k, indicating that the training set of “graffiti” in

ImageNet21k has little overlap with the graffiti on freight cars. Finally, we note that the better performance for models fine-tuned from ImageNet21k implies only that the reliance on the 40 spurious features has improved, but it could be that ImageNet21k introduces novel spurious features.

6.3. Mitigation of spurious features

Fixing spurious features is a non-trivial task and can require substantial labeling effort. We test the technique from Sec. 5 where one replaces $\alpha_l^{(k)}$ with $\min\{\alpha_l^{(k)}, 0\}$ in the expression for the logit, see (8). No retraining or fine-tuning is required. The strong effect of this fix of spurious features (SpuFix) can be seen in Tab. 1 and Fig. 5. Compared to our original robust ResNet50 with a spurious mAUC of 0.629, the SpuFix version has a spurious mAUC of 0.781 which reaches almost the level of the ConvNext-B with 0.791. Test set accuracy reduces by 0.6% but this is a rather positive effect, as several of the additional errors are because the robust ResNet50 uses spurious features for its decision e.g., for classes like “balance beam” or “puck” the class object is often not even visible in the cropped test set images.

7. Conclusion

We have shown that a large-scale identification of spurious features is feasible with our neural PCA components and neural PCA feature visualizations. We introduced a new validation technique together with our “Spurious ImageNet” dataset which allows evaluating the dependence of ImageNet classifiers on a set of spurious features based on real images which we think should become a standard measure besides test set performance.

References

- [1] Julius Adebayo, Michael Muelly, Hal Abelson, and Been Kim. Post hoc explanations may be ineffective for detecting unknown spurious correlation. In *ICLR*, 2022. 2
- [2] Julius Adebayo, Michael Muelly, Ilaria Lliccardi, and Been Kim. Debugging tests for model explanations. In *NeurIPS*, 2020. 1, 2
- [3] D. Amodei, C. Olah, J. Steinhardt, P. Christiano, J. Schulman, and D. Mane. Concrete problems in AI safety. arXiv:1606.06565v2, 2016. 2
- [4] Christopher J. Anders, Leander Weber, David Neumann, Wojciech Samek, Klaus-Robert Müller, and Sebastian Lapuschkin. Finding and removing clever hans: Using explanation methods to debug and improve deep models. *Information Fusion*, 77:261–295, 2022. 2
- [5] Maximilian Augustin, Valentyn Boreiko, Francesco Croce, and Matthias Hein. Diffusion visual counterfactual explanations. In *NeurIPS*, 2022. 2, 11, 15, 24
- [6] Maximilian Augustin, Alexander Meinke, and Matthias Hein. Adversarial robustness on in- and out-distribution improves explainability. In *ECCV*, 2020. 2, 3
- [7] David Baehrens, Timon Schroeter, Stefan Harmeling, Motoaki Kawanabe, Katja Hansen, and Klaus-Robert Müller. How to explain individual classification decisions. *JMLR*, 2010. 2
- [8] Sara Beery, Grant van Horn, and Pietro Perona. Recognition in terra incognita. In *ECCV*, 2018. 2
- [9] Lucas Beyer, Olivier J Hénaff, Alexander Kolesnikov, Xiaoahua Zhai, and Aäron van den Oord. Are we done with ImageNet? arXiv:2006.07159, 2020. 2
- [10] B. Biggio, I. Corona, D. Maiorca, B. Nelson, N. Srndic, P. Laskov, G. Giacinto, and F. Roli. Evasion attacks against machine learning at test time. In *ECML/PKDD*, 2013. 2
- [11] Alceu Bissoto, Eduardo Valle, and Sandra Avila. Debiasing skin lesion datasets and models? not so fast. arXiv:2004.11457, 2020. 2
- [12] Valentyn Boreiko, Maximilian Augustin, Francesco Croce, Philipp Berens, and Matthias Hein. Sparse visual counterfactual explanations in image space. In *GCPR*, 2022. 2, 3
- [13] Tom Brown, Benjamin Mann, Nick Ryder, Melanie Subbiah, Jared D Kaplan, Prafulla Dhariwal, Arvind Neelakantan, Pranav Shyam, Girish Sastry, Amanda Askell, Sandhini Agarwal, Ariel Herbert-Voss, Gretchen Krueger, Tom Henighan, Rewon Child, Aditya Ramesh, Daniel Ziegler, Jeffrey Wu, Clemens Winter, Chris Hesse, Mark Chen, Eric Sigler, Mateusz Litwin, Scott Gray, Benjamin Chess, Jack Clark, Christopher Berner, Sam McCandlish, Alec Radford, Ilya Sutskever, and Dario Amodei. Language models are few-shot learners. In *NeurIPS*, 2020. 1
- [14] Myung Jin Choi, Antonio Torralba, and Alan S. Willsky. Context models and out-of-context objects. *Pattern Recognition Letters*, 33(7):853–862, 2012. 2
- [15] Francesco Croce and Matthias Hein. Reliable evaluation of adversarial robustness with an ensemble of diverse parameter-free attacks. In *ICML*, 2020. 4
- [16] Prafulla Dhariwal and Alex Nichol. Diffusion models beat gans on image synthesis. In *NeurIPS*, 2021. 2
- [17] Ann-Kathrin Dombrowski, Maximillian Alber, Christopher Anders, Marcel Ackermann, Klaus-Robert Müller, and Pan Kessel. Explanations can be manipulated and geometry is to blame. In *NeurIPS*, 2019. 2
- [18] Logan Engstrom, Andrew Ilyas, Shibani Santurkar, Dimitris Tsipras, Brandon Tran, and Aleksander Madry. Adversarial robustness as a prior for learned representations, 2019. 4
- [19] Christian Etmann, Sebastian Lunz, Peter Maass, and Carola-Bibiane Schönlieb. On the connection between adversarial robustness and saliency map interpretability. In *ICML*, 2019. 2, 3
- [20] Robert Geirhos, Jörn-Henrik Jacobsen, Claudio Michaelis, Richard Zemel, Wieland Brendel, Matthias Bethge, and Felix A. Wichmann. Shortcut learning in deep neural networks. *Nature Machine Intelligence*, 2(11):665–673, 2020. 1, 2
- [21] R. Geirhos, P. Rubisch, C. Michaelis, M. Bethge, F. A. Wichmann, and W. Brendel. Imagenet-trained cnns are biased towards texture; increasing shape bias improves accuracy and robustness. In *ICLR*, 2019. 2
- [22] Amirata Ghorbani, Abubakar Abid, and James Zou. Interpretation of neural networks is fragile. In *AAAI*, 2019. 2
- [23] M. Hein, M. Andriushchenko, and J. Bitterwolf. Why ReLU networks yield high-confidence predictions far away from the training data and how to mitigate the problem. In *CVPR*, 2019. 1, 2
- [24] D. Hendrycks and T. Dietterich. Benchmarking neural network robustness to common corruptions and perturbations. In *ICLR*, 2019. 1, 2
- [25] D. Hendrycks and K. Gimpel. A baseline for detecting misclassified and out-of-distribution examples in neural networks. In *ICLR*, 2017. 1, 2
- [26] Jonathan Ho and Tim Salimans. Classifier-free diffusion guidance. In *NeurIPS Workshop*, 2021. 2
- [27] Sara Hooker, Yann Dauphin, Aaron Courville, and Andrea Frome. Selective brain damage: Measuring the disparate impact of model pruning. In *ICLR*, 2020. 2
- [28] Pieter Abbeel Jonathan Ho, Ajay Jain. Denoising diffusion probabilistic models. In *NeurIPS*, 2020. 2
- [29] A. Kurakin, I. J. Goodfellow, and S. Bengio. Adversarial examples in the physical world. In *ICLR Workshop*, 2017. 1
- [30] Alina Kuznetsova, Hassan Rom, Neil Alldrin, Jasper Uijlings, Ivan Krasin, Jordi Pont-Tuset, Shahab Kamali, Stefan Popov, Matteo Mallocci, Alexander Kolesnikov, Tom Duerig, and Vittorio Ferrari. The open images dataset v4: Unified image classification, object detection, and visual relationship detection at scale. *IJCV*, 2020. 7
- [31] Scott M. Lundberg and Su-In Lee. A unified approach to interpreting model predictions. In *NeurIPS*, 2017. 2
- [32] Aleksander Madry, Aleksandar Makelov, Ludwig Schmidt, Dimitris Tsipras, and Adrian Vladu. Towards deep learning models resistant to adversarial attacks. In *ICLR*, 2018. 2
- [33] Mazda Moayeri, Sahil Singla, and Soheil Feizi. Hard ImageNet: Segmentations for objects with strong spurious cues. In *NeurIPS Datasets and Benchmarks Track*, 2022. 2, 7
- [34] A. Nguyen, J. Yosinski, and J. Clune. Deep neural networks are easily fooled: High confidence predictions for unrecognizable images. In *CVPR*, 2015. 1, 2

- [35] Gregory Plumb, Marco Tulio Ribeiro, and Ameet Talwalkar. Finding and fixing spurious patterns with explanations. *Transactions on Machine Learning Research (TMLR)*, 2022. [2](#), [7](#)
- [36] Benjamin Recht, Rebecca Roelofs, Ludwig Schmidt, and Vaishaal Shankar. Do ImageNet classifiers generalize to ImageNet? In *ICML*, 2019. [1](#)
- [37] Marco Tulio Ribeiro, Sameer Singh, and Carlos Guestrin. "why should i trust you?": Explaining the predictions of any classifier. In *KDD*, 2016. [2](#)
- [38] Olga Russakovsky, Jia Deng, Hao Su, Jonathan Krause, Sanjeev Satheesh, Sean Ma, Zhiheng Huang, Andrej Karpathy, Aditya Khosla, Michael Bernstein, Alexander C. Berg, and Li Fei-Fei. Imagenet large scale visual recognition challenge. *IJCV*, 2015. License: No license specified. [2](#)
- [39] Shibani Santurkar, Dimitris Tsipras, Brandon Tran, Andrew Ilyas, Logan Engstrom, and Aleksander Madry. Image synthesis with a single (robust) classifier. In *NeurIPS*, 2019. [2](#), [3](#)
- [40] Kathryn Schutte, Olivier Moindrot, Paul Hérent, Jean-Baptiste Schiratti, and Simon Jégou. Using stylegan for visual interpretability of deep learning models on medical images. In *NeurIPS Workshop*, 2020. [2](#)
- [41] Ramprasaath R. Selvaraju, Michael Cogswell, Abhishek Das, Ramakrishna Vedantam, Devi Parikh, and Dhruv Batra. Grad-cam: Visual explanations from deep networks via gradient-based localization. In *ICCV*, 2017. [2](#), [3](#), [5](#)
- [42] Harshay Shah, Kaustav Tamuly, Aditi Raghunathan, Prateek Jain, and Praneeth Netrapalli. The pitfalls of simplicity bias in neural networks. In *NeurIPS*, 2020. [2](#)
- [43] Rakshith Shetty, Bernt Schiele, and Mario Fritz. Not using the car to see the sidewalk—quantifying and controlling the effects of context in classification and segmentation. In *CVPR*, 2019. [2](#), [7](#)
- [44] Krishna Kumar Singh, Dhruv Mahajan, Kristen Grauman, Yong Jae Lee, Matt Feiszli, and Deepti Ghadiyaram. Don't judge an object by its context: learning to overcome contextual bias. In *CVPR*, 2020. [2](#)
- [45] Sahil Singla and Soheil Feizi. Salient imagenet: How to discover spurious features in deep learning? In *ICLR*, 2022. [1](#), [2](#), [3](#), [4](#), [5](#), [7](#), [8](#), [11](#), [12](#), [14](#), [20](#), [21](#)
- [46] Sahil Singla, Mazda Moayeri, and Soheil Feizi. Core risk minimization using salient imagenet. *arXiv:2203.15566*, 2022. [2](#), [5](#), [7](#), [8](#)
- [47] Sahil Singla, Besmira Nushi, Shital Shah, Ece Kamar, and Eric Horvitz. Understanding failures of deep networks via robust feature extraction. In *CVPR*, 2021. [4](#)
- [48] Dylan Slack, Sophie Hilgard, Emily Jia, Sameer Singh, and Himabindu Lakkaraju. Fooling lime and shap: Adversarial attacks on post hoc explanation methods. In *Proceedings of the AAAI/ACM Conference on AI, Ethics, and Society*, pages 180–186, 2020. [2](#)
- [49] Yang Song, Conor Durkan, Iain Murray, and Stefano Ermon. Maximum likelihood training of score-based diffusion models. In *NeurIPS*, 2021. [2](#)
- [50] Yang Song, Jascha Sohl-Dickstein, Diederik P Kingma, Abhishek Kumar, Stefano Ermon, and Ben Poole. Score-based generative modeling through stochastic differential equations. In *ICLR*, 2021. [2](#)
- [51] Pierre Stock and Moustapha Cisse. Convnets and ImageNet beyond accuracy: Understanding mistakes and uncovering biases. In *ECCV*, 2018. [2](#)
- [52] Christian Szegedy, Wojciech Zaremba, Ilya Sutskever, Joan Bruna, Dumitru Erhan, Ian Goodfellow, and Rob Fergus. Intriguing properties of neural networks. In *ICLR*, 2014. [1](#), [2](#)
- [53] Antonio Torralba and Alexei A Efros. Unbiased look at dataset bias. In *CVPR*, pages 1521–1528, 2011. [2](#)
- [54] Dimitris Tsipras, Shibani Santurkar, Logan Engstrom, Andrew Ilyas, and Aleksander Madry. From ImageNet to image classification: Contextualizing progress on benchmarks. In *ICML*, 2020. [2](#)
- [55] Dimitris Tsipras, Shibani Santurkar, Logan Engstrom, Alexander Turner, and Aleksander Madry. Robustness may be at odds with accuracy. In *ICLR*, 2019. [3](#)
- [56] Sahil Verma, John P. Dickerson, and Keegan Hines. Counterfactual explanations for machine learning: A review. *arXiv:2010.10596*, 2020. [2](#)
- [57] Sandra Wachter, Brent Mittelstadt, and Chris Russell. Counterfactual explanations without opening the black box: Automated decisions and the GDPR. *Harvard Journal of Law & Technology*, 2018. [2](#)
- [58] Eric Wong, Shibani Santurkar, and Aleksander Madry. Leveraging sparse linear layers for debuggable deep networks. In *ICML*, 2021. [2](#)
- [59] Kai Yuanqing Xiao, Logan Engstrom, Andrew Ilyas, and Aleksander Madry. Noise or signal: The role of image backgrounds in object recognition. In *ICLR*, 2021. [2](#)
- [60] John R. Zech, Marcus A. Badgeley, Manway Liu, Anthony B. Costa, Joseph J. Titano, and Eric Karl Oermann. Variable generalization performance of a deep learning model to detect pneumonia in chest radiographs: A cross-sectional study. *PLOS Medicine*, 15(11):1–17, 2018. [1](#), [2](#)
- [61] Zhuotun Zhu, Lingxi Xie, and Alan L. Yuille. Object recognition with and without objects. In *IJCAI*, 2017. [2](#)

Overview of Appendix

In the following, we provide a brief overview of the additional experiments reported in the Appendix.

- In App. A, we compare our Neural PCA components vs. the neural features of the top 5 neurons introduced in [45] for classes “Koala”, “Indigo-Bunting”, and “Mountain Bike”, for which [45] do not find spurious features and we do.
- In App. B, we explain in more detail our labeling setup to create the dataset “Spurious ImageNet”.
- In App. C, we extend our qualitative evaluation of the spurious components from Figure 4.
- In App. D, we show random samples from our “Spurious ImageNet” dataset.
- In App. E, we use our “Spurious ImageNet” dataset to quantitatively analyze the dependence of the classifiers on spurious components. By doing so, we show that pre-training on ImageNet21k helps to reduce this dependence.
- In App. F, we show how we change the predicted class for an image by introducing only spurious features of the target class. To do this automatically, we adapt the Diffusion Visual Counterfactual Explanations (DVCEs) of [5].

A. Neural PCA Components

Here, we illustrate in Fig. 6 that our neural PCA components capture better the different subpopulations in the training set compared to the neural features of [45]. We find three spurious features: eucalyptus/plants for the class koala, twigs for the class indigo bunting, and forest for mountain bike, which were not found by [45]. Please see the caption of Fig. 6 for more details.

From the 40 classes in our “Spurious ImageNet” dataset, for eleven of them no spurious feature is reported in [45]. The eleven classes are: tench, indigo bunting, sulphur-crested cockatoo, koala, walking stick, gar, freight car, hard disc, mountain bike, quill, radio telescope.

B. Labeling Setup for Spurious features

In our paper, we have 2 labeling tasks for 2 objectives: i) identifying spurious components, and ii) creating “Spurious ImageNet”.

Identifying spurious components. Fig. 7 illustrates the information shown to the human labeler to identify neural PCA components corresponding to spurious features. This includes the NPFV, the 5 most activating training images, and GradCAM heatmaps, as well as the corresponding class

probabilities and $\alpha_l^{(k)}$ values. The decision, of whether a neural PCA component corresponds to a spurious feature has been made only based on the visualization as shown in Fig. 7.

Creating “Spurious ImageNet”. In order to create our “Spurious ImageNet” dataset,

- we selected 40 (spurious component l , class k) pairs, such that for each class we have only one selected spurious component, and sorted all images from OpenImages for which at least two of our four classifiers predict class k according to the value of the respective neural PCA component $\alpha_l^{(k)}$;
- we have used the open-source tool² for labeling images and created three labels “in” (the images that contain the class features), “out” (the images that contain only the spurious and no class features), “trash” (images that are too far from the distribution of the spurious features and contain no class features) for each image as can be seen in the Fig. 8;
- for each component, 75 images that are guaranteed to contain the spurious feature but not the class object of class k were selected by two human labelers. Images were only accepted into the dataset if both labelers assigned the label “out”.

C. Extended Qualitative Evaluation

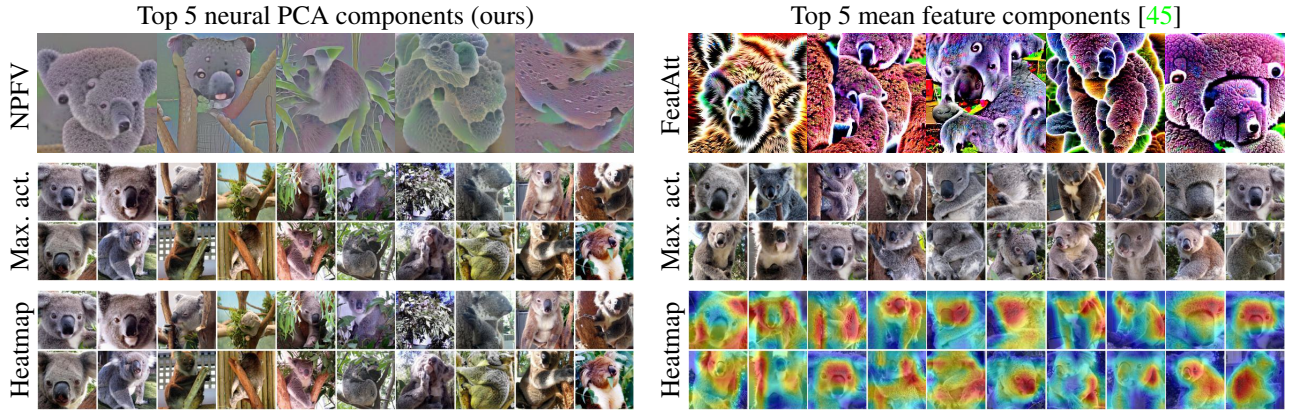
Here, we extend our qualitative evaluation of the found harmful spurious components from Figure 4. Concretely, for each such pair (class k , component l) we show in Fig. 9 and 10: i) random training images from class k , ii) NPFV of the component l together with the most activating images of $\alpha_l^{(k)}$, and iii) examples of images that display only the spurious feature but no class features and are **incorrectly** classified by four ImageNet classifiers as class k .

D. Random samples from our “Spurious ImageNet” dataset

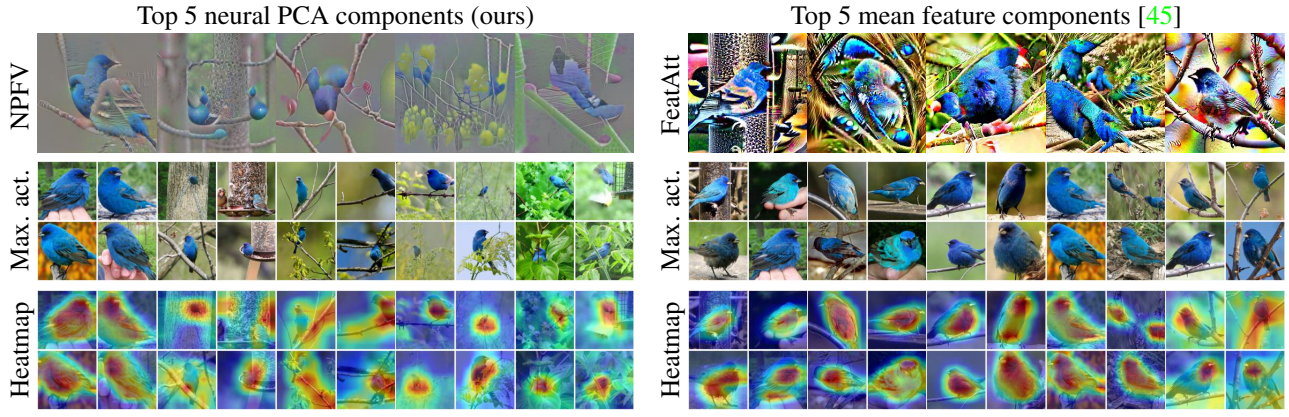
To visualize our “Spurious ImageNet” dataset, for each of the 40 classes in our dataset, we show 4 randomly drawn images (out of the 75 int total) in Fig. 11 and 12. We also provide a label for the spurious feature shown in brackets. We again highlight that none of the images contains the actual class object.

²<https://github.com/robertbrada/PyQt-image-annotation-tool>

Koala



Indigo Bunting



Mountain Bike

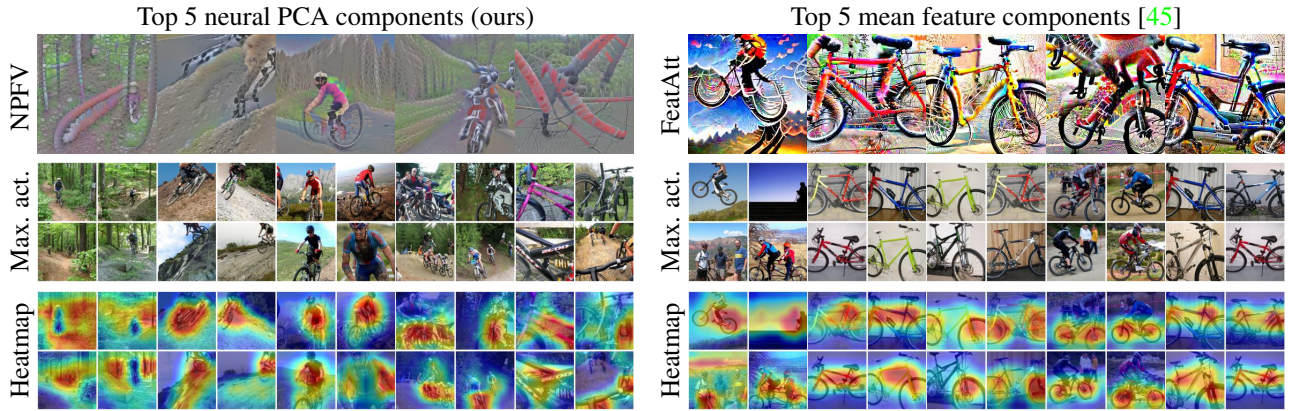


Figure 6. **Neural PCA feature components vs neural features of [45] for class hummingbird:** The first row shows our neural PCA feature visualization (NPFV) of our top 5 neural PCA components (left), and the feature attacks of the top 5 neurons of [45] (right). The second row shows the four most activating training images of the components/neurons and the last row GradCAM for the neural PCA components (left) and the neural activation map of [45] (right). For these three classes [45] report no spurious feature. As in Figure 3 our neural PCA components are capturing different subpopulations in the training data. Our neural PCA Component 3 of Koala shows prominent leaves in the NPFV and neural PCA GradCAM heatmaps and is identified as spurious, similar for our component 3 of Indigo Bunting showing twigs in the NPFV and activated in the heatmap, and component 1 for mountain bike where the forest appears in the NPFV and is active in the heatmap. The feature attack of [45] produces an image similar to the most activating training image and thus does not add new information, whereas our NPFV allows to identify which features the component has picked up.

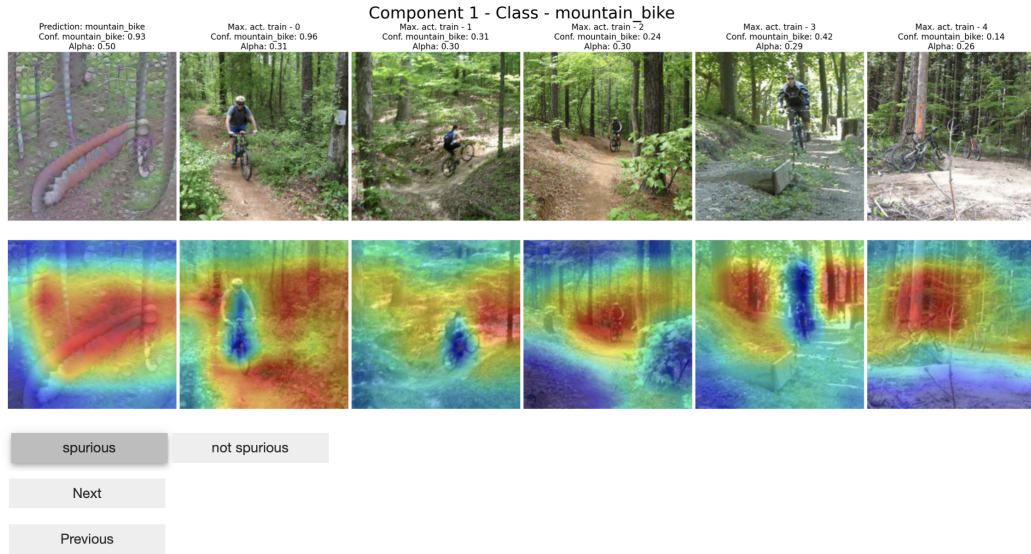


Figure 7. **Illustration of the information shown for labeling neural PCA components:** The illustration shows the visualization of the first neural PCA component of the class “mountain bike”. The first image on the left shows the NPFV, the prediction of the robust ResNet50, its probability for the class “mountain bike”, and the corresponding value of $\alpha_l^{(k)}$. The other five images shown, along with the corresponding probabilities and $\alpha_l^{(k)}$, are the maximally activating training images of this component. The second row shows GradCAM heatmaps with respect to the component $\alpha_l^{(k)}(x)$. Below the visualization, the labeler can select one of the two possible labels (*spurious* and *not spurious*) and navigate through the next or last neural PCA component.

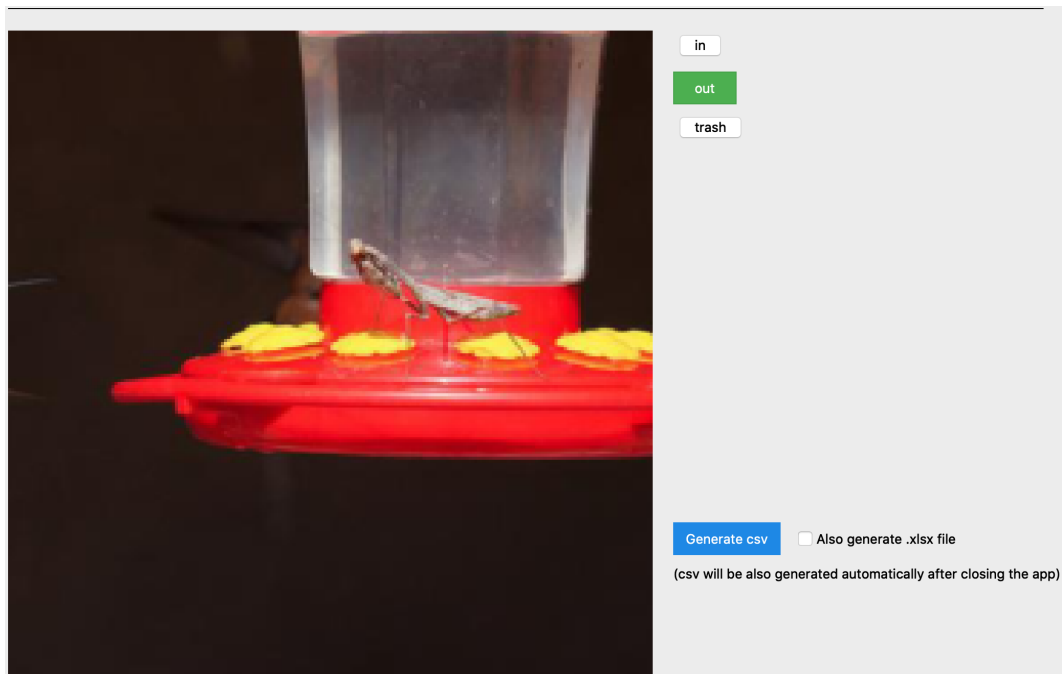


Figure 8. **Illustration of the information shown for labeling images to create our “Spurious ImageNet”:** This screenshot illustrates a tool that we used to create labels for our dataset and an example of the image that is chosen to be in our dataset, in class “hummingbird”, as it contains the spurious feature bird feeder of the class “hummingbird” but no hummingbird.

E. Quantitative Evaluation

In the following Section, we extend the quantitative results given in the main paper in Tab. 1 for a selection of ImageNet models. In Tab. 2 we show ILSVRC-2012 test accuracies and the mean spurious AUC (mAUC) for a wide selection of ImageNet models with different architectures and training configurations. Again, our spurious AUC is computed classwise using the predicted probability for that class as score where we compare the images corresponding to this class of “Spurious ImageNet” (not showing the class object, but just the spurious feature) vs the ImageNet validation set images of that class. Finally, we take the mean of all classwise AUCs to get the final mAUC. All models except for our multiple-norm robust ResNet50, the robust ResNet50 from [45] and our SpuFix are taken from PyTorch Image Models³.

In Tab. 2, we further distinguish between models trained on ImageNet1k only (in1k), models pre-trained on ImageNet21k and then fine-tuned on ImageNet1k (in1kFT21k), and ImageNet21k classifiers (in21k). Note that we do not report accuracies for the last category of models as no test set for in21k is available. In Fig. 13, we also plot mean spurious AUC against ImageNet-1k test accuracy and color code the models based on the dataset used during training.

Overall, the trend seems to be that better models (in terms of accuracy) typically also improve in mAUC and are less vulnerable to spurious features. It is also easily observable that pre-training on larger datasets such as ImageNet-21k can help to decrease vulnerability to spurious features, which can be seen best from the EfficientNetv2-M/L and ConvNeXt-L models for which we can evaluate the difference between in1k, in1kFT21k, and in21k training. The in1k EfficientNetv2-L achieves an mAUC of 0.85 whereas the same in21k model achieves an mAUC of 0.93. However, it is important to note that the mAUC decreases again for the in1kFT21k model to 0.89 during fine-tuning. Similar trends are also visible for the EfficientNetv2-M and ConvNeXt-L models, where all ImageNet21k models (in1kFT21k and in21k) perform better than pure in1k models, however, we lose part of our mAUC improvement during fine-tuning. While we do not have pure in1k models for them to compare to, other in21k pre-trained models such as the Big Transfer models, as well as the ViT and BeiT architecture-based models show the same behavior and decrease spurious mAUC during fine-tuning. It thus remains an open question how one can use the benefits of pre-training on massive datasets with fine-grained class structures to preserve or even improve mAUC during fine-tuning to smaller datasets such as ImageNet1k. In terms of architecture, there is no easily observable trend. On pure in1k mod-

els, VOLO D5 achieves the best mAUC of 0.87, however, it is also by far the most accurate model, beating the EfficientNetv2-L by 1.5% in terms of accuracy. The best overall model in terms of mAUC is the ConvNeXt-XL in21k with a mAUC of 0.95, however, after fine-tuning, the vision transformer ViT-L with input resolution 384px overtakes the finetuned ConvNeXt (0.93 vs 0.90) and is the best model with ImageNet-1k classification head in terms of mAUC. In summary, attention-based transformers do not seem to yield strong benefits over convolutional neural networks in terms of vulnerability to spurious features.

While the general trend of accuracy vs mAUC validates the progress of recent vision models, it does not mean that spurious features are no longer a problem for those models, especially since the worst-performing classes are still severe modes of failure. To better understand this behavior on individual classes, we plot the class-wise AUC for all 40 classes and a selection of models in Fig. 14 and 15. While both robust ResNet50 models are overall worse than the much larger comparison models EfficientNetv2-L and ConvNeXt-L, we highlight that our SpuFix method (see Section 6.3) does significantly improve the mean spurious AUC of our robust ResNet50 without requiring retraining. On average, it is again observable that ImageNet-21k pre-training does improve spurious AUC. However, in terms of the final ImageNet-1k classifier after fine-tuning, classes like snorkel, flagpole, pot, or pole remain challenging and can have a class-wise AUC as low as 0.5. Thus the improvements seem to depend heavily on the structure of the dataset used for pretraining and whether or not this dataset contains the spurious feature as an individually labeled class that allows the model to distinguish the class object from the spurious feature. For example, ImageNet-21k contains both flagpole and flag as separate classes, thus the in21k EfficientNet and ConvNeXt models achieve much better spurious AUC for that class (Spurious ImageNet contains flag images without flagpoles) than models with an ImageNet-1k classification head. Nevertheless, even the in21k models still show a low AUC for flag pole and thus have huge problems to distinguish between flags (spurious feature) and flag pole. It also has to be noticed that the seemingly high AUC values are sometimes misleading. First, of all we stress again that the images of Spurious ImageNet do not contain the class object and thus an AUC of one should be easily obtainable for a classifier. Second, even if the AUC is one, it only means that the predicted probability for the validation set images (containing the class object) is always higher than the predicted probability for images from Spurious ImageNet (not containing the class object). However, still a large fraction of the Spurious ImageNet images can be classified as the corresponding class, e.g. the ConvNeXt-L-1kFT21k has a class-wise AUC of 0.929 for “quill”, but still 76% of all Images from Spurious ImageNet are classi-

³PyTorch Image Models [https://github.com/rwightman/pytorch-image-models]

fied as “quill”, see Fig. 16 where we show for each image from “Spurious ImageNet” the top-3 predictions with their predicted probabilities. Thus the class-extension can still be significant even for such a strong model. There are also classes which are completely broken like puck with an AUC of 0.69, where 100% of all images in “Spurious ImageNet” are classified as puck. The reason is that the puck is simply too small in the image (or sometimes even not visible at all), whereas the ice hockey players and also part of the playing field boundary are the main objects in the image. Thus the classification is only based on spurious features and the object “puck” has never been learned at all.

F. Adding spurious features changes the prediction of classifier

In this section we show how one can adapt the recent method “Diffusion Visual Counterfactual Explanations” [5] to generate the spurious feature on a given image without changing the overall structure of the image. We first introduce the necessary notation. We denote by $n(x) = \frac{x}{\|x\|_2}$ for $x \neq 0$, the normalization of a vector by its l_2 norm and the confidence of the Rob. ResNet50 classifier in a target class k as

$$p_{\text{robust},\psi} : [0, 1]^d \rightarrow (0, 1), \quad x \mapsto \frac{e^{f_{\text{robust},\psi,k}(x)}}{\sum_{i=1}^K e^{f_{\text{robust},\psi,i}(x)}}.$$

Here, $f_{\text{robust},\psi} : [0, 1]^d \rightarrow \mathbb{R}^K$ are the logits of the robust classifier, and $f_{\text{robust},\psi,k}(x)$ denotes the logit of class k .

To automatically add spurious features to any given image, we adapt a recently proposed method Diffusion Visual Counterfactual Explanations (DVCEs) [5], where at a step t the shifted mean μ_t is of the form

$$\begin{aligned} g_{\text{update}} &= C_c g_c - C_d g_d + C_a g_a, \\ \mu_t &= \mu_\theta(x_t, t) + \Sigma_\theta(x_t, t) \|\mu_\theta(x_t, t)\|_2 g_{\text{update}}, \\ p(x_{t-1}|x_t, \hat{x}, k) &= \mathcal{N}(\mu_t, \Sigma_\theta(x_t, t)), \end{aligned}$$

where $g_c := n(\nabla_{x_t} \log p_{\text{robust},\psi}(k|f_{\text{dn}}(x_t, t)))$ is the normalized gradient of the adversarially robust classifier, $g_d := n(\nabla_{x_t} d(\hat{x}, f_{\text{dn}}(x_t, t)))$ - normalized gradient of the distance term. We add as additional guidance $g_a := n(\nabla_{x_t} \alpha_j^{(k)}(f_{\text{dn}}(x_t, t)))$ - the normalized gradient of the contribution $\alpha_j^{(k)}$ of the j -th neural PCA component to the logit of class k . As the derivative of the diffusion models, relies on noisy updates, and classifier Rob. ResNet50 has not been trained on such inputs, [5] propose to use as an input to the classifier the denoised sample $\hat{x}_0 = f_{\text{dn}}(x, t)$ of the noisy input x_t . Intuitively, at every step t of the generative denoising process, the method of [5] follows i) the direction g_a that increases the contribution of neural PCA component j (corresponding to a desired spurious feature)

of class k to the logit $f_k(x)$ of this class, ii) the direction g_c that increases the confidence of the classifier in the class k , and iii) the direction g_d that decreases the distance to the original image \hat{x} .

In our experiments, we set $d(x, y) := \|x - y\|_1$ following [5] and coefficients as follows: $C_c = 0.1, C_d = 0.35, C_a = 0.05$. With these parameters, we generate the desired DVCEs in Fig. 17. There, using minimal realistic perturbations to the original image we can change the prediction of the classifier in the target class k with high confidence. Moreover, these perturbations introduce only *harmful* spurious features to the image and not class-specific features e.g. for freight car the DVCE generates graffiti but no features of a freight car.

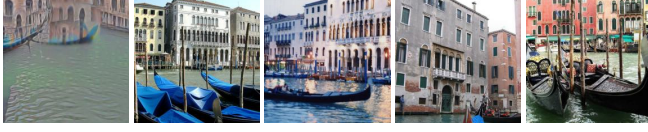
This happens, because, as has been shown qualitatively in Fig. 4 and quantitatively in Fig. 5, this classifier has learned to associate class “fireboat” with the spurious feature “water jet”, “freight car” - with “graffiti”, “flagpole” with a flag without the pole and mostly with “US flag”, and “hard disc” - with “label”, and therefore introducing only these *harmful* spurious features is enough to increase the confidence in the target class k significantly.

Gondola - Random train. images (**confidence** / α_k)



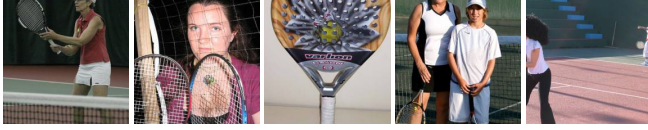
1.00/3.2 1.00/0.6 0.98/-3.8 1.00/1.2 0.98/-2.0

NPFV-1 Max. activating train. images - N-PCA Comp. 1



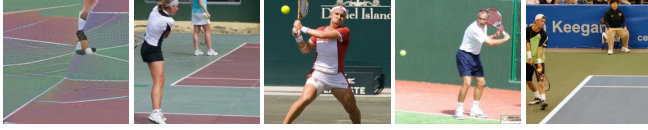
1.00/6.9 1.00/7.7 1.00/6.9 0.96/6.9 1.00/6.9

Racket - Random train. images (**confidence** / α_k)



0.93/0.7 0.38/-3.0 0.62/-2.4 0.12/-3.1 0.97/2.1

NPFV-5 Max. activating train. images - N-PCA Comp. 5



1.00/17.8 0.78/7.5 1.00/7.2 1.00/7.0 1.00/7.0

Dam - Random train. images (**confidence** / α_k)



0.44/0.1 0.52/0.1 0.28/0.0 1.00/-0.0 0.85/-0.0

NPFV-1 Max. activating train. images - N-PCA Comp. 1



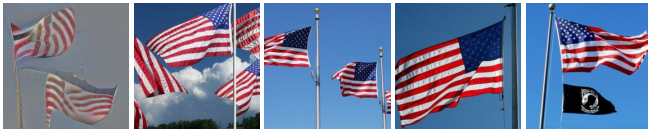
1.00/0.2 1.00/0.1 0.97/0.1 1.00/0.1 0.70/0.1

Flagpole - Random train. images (**confidence** / α_k)



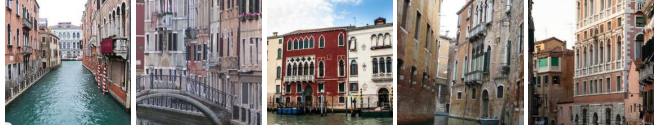
1.00/4.9 0.25/-3.9 1.00/5.4 0.86/-0.4 0.99/-1.3

NPFV-1 Max. activating train. images - N-PCA Comp. 1



1.00/16.1 1.00/11.6 1.00/11.1 1.00/10.8 1.00/10.8

Images with spurious **houses/river** but **no gondola**



0.92/6.4 0.82/4.4 0.73/3.1 0.85/4.9 0.82/4.1

all classified as **gondola** by four ImageNet models



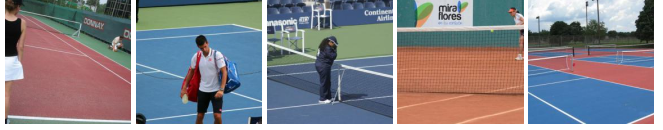
0.88/4.5 0.90/5.7 0.74/5.4 0.79/5.6 0.90/5.6

Images with spurious **tennis court/player** but **no racket**



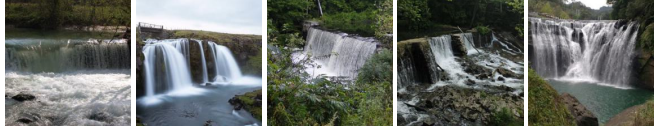
0.82/6.2 0.94/4.3 0.90/3.8 0.97/3.7 0.76/5.9

all classified as **racket** by four ImageNet models



0.94/5.7 0.83/4.7 0.76/4.2 0.90/3.8 0.56/3.8

Images with spurious **waterfall** but **no dam**



0.30/0.1 0.99/0.1 0.67/0.1 0.55/0.1 0.99/0.1

all classified as **dam** by four ImageNet models



0.55/0.1 0.63/0.1 0.62/0.1 0.76/0.1 0.77/0.1

Images with spurious **US flag** but **no flag pole**



1.00/8.3 0.98/3.6 0.96/6.6 0.38/3.4 0.99/5.4

all classified as **flag pole** by four ImageNet models



0.94/5.1 1.00/6.6 0.99/5.1 1.00/8.8 0.75/4.2

Figure 9. **Spurious features (ImageNet)**: found by human labeling of our neural PCA components. For each class we show 5 random train. images (top left), the neural PCA Feature Visual. (NPFV) and 4 most activating train. images for the spurious feature component (bottom left). Right: four ImageNet models classify images **showing only the spurious feature but no class object** as this class.

Hard disc - Random train. images (confidence / α_k)



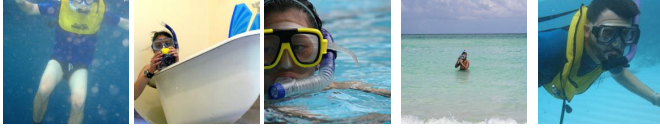
0.93/0.3 0.03/-3.3 1.00/0.7 0.04/-0.32 0.97/-0.3

NPFV-1 Max. activating train. images - N-PCA Comp. 1



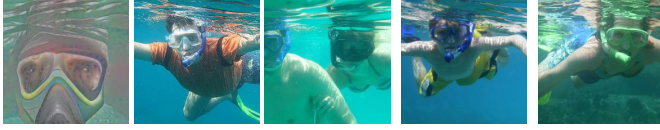
1.00/14.0 1.00/9.8 1.00/8.8 1.00/8.3 1.00/8.3

Snorkel - Random train. images (confidence / α_k)



0.67/-0.1 0.01/-3.8 1.00/2.4 0.17/-2.3 0.84/1.8

NPFV-1 Max. activating train. images - N-PCA Comp. 1



1.00/9.6 1.00/6.9 1.00/5.9 1.00/5.9 0.97/5.8

Mountain bike - Random train. images (confidence / α_k)



0.46/-0.2 0.70/0.1 0.99/0.1 0.00/0.0 0.55/-0.1

NPFV-1 Max. activating train. images - N-PCA Comp. 1



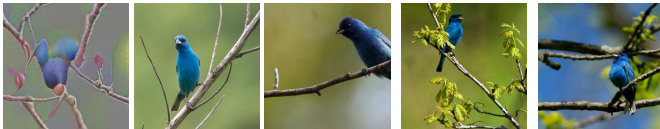
0.93/0.5 0.96/0.3 0.31/0.3 0.24/0.3 0.42/0.3

Indigo Bunting - Random train. images (confidence / α_k)



1.00/2.1 0.00/-2.1 1.00/-1.1 1.00/1.2 1.00/0.4

NPFV-3 Max. activating train. images - N-PCA Comp. 3



1.00/7.7 1.00/3.8 0.98/3.6 1.00/3.6 0.98/3.5

Images with spurious (serial) labels but no hard disc



0.74/6.6 0.66/6.5 0.68/5.75 0.62/5.4 0.65/5.3

all classified as **hard disc** by four ImageNet models



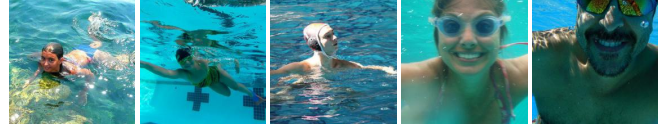
0.85/4.9 0.59/4.6 0.72/4.3 0.83/3.9 0.53/3.9

Images with spurious diver/human but no snorkel



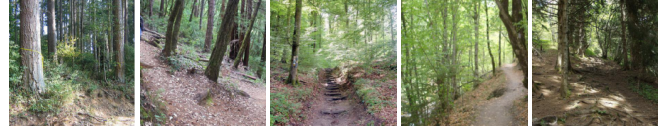
0.90/5.0 0.64/4.3 0.83/3.8 0.64/3.8 0.74/3.3

all classified as **snorkel** by four ImageNet models



0.71/3.1 0.61/3.1 0.59/3.0 0.59/2.8 0.55/2.8

Images with spurious forest but no mountain bike



0.31/0.3 0.60/0.3 0.33/0.3 0.36/0.3 0.35/0.3

all classified as **mountain bike** by four ImageNet models



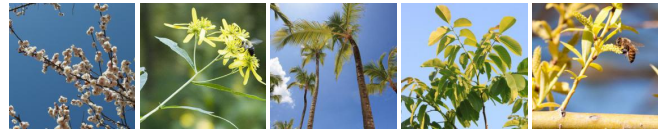
0.45/0.3 0.37/0.3 0.34/0.3 0.52/0.3 0.53/0.3

Images with spurious twigs but no indigo bunting



0.56/2.8 0.49/2.4 0.30/2.4 0.16/2.3 0.35/2.2

all classified as **indigo bunting** by four ImageNet models



0.36/2.2 0.37/2.1 0.50/1.8 0.44/1.8 0.55/1.7

Figure 10. **Spurious features (ImageNet):** found by human labeling of our neural PCA components. For each class we show 5 random train. images (top left), the neural PCA Feature Visual. (NPFV) and 4 most activating train. images for the spurious feature component (bottom left). Right: four ImageNet models classify images **showing only the spurious feature but no class object** as this class.

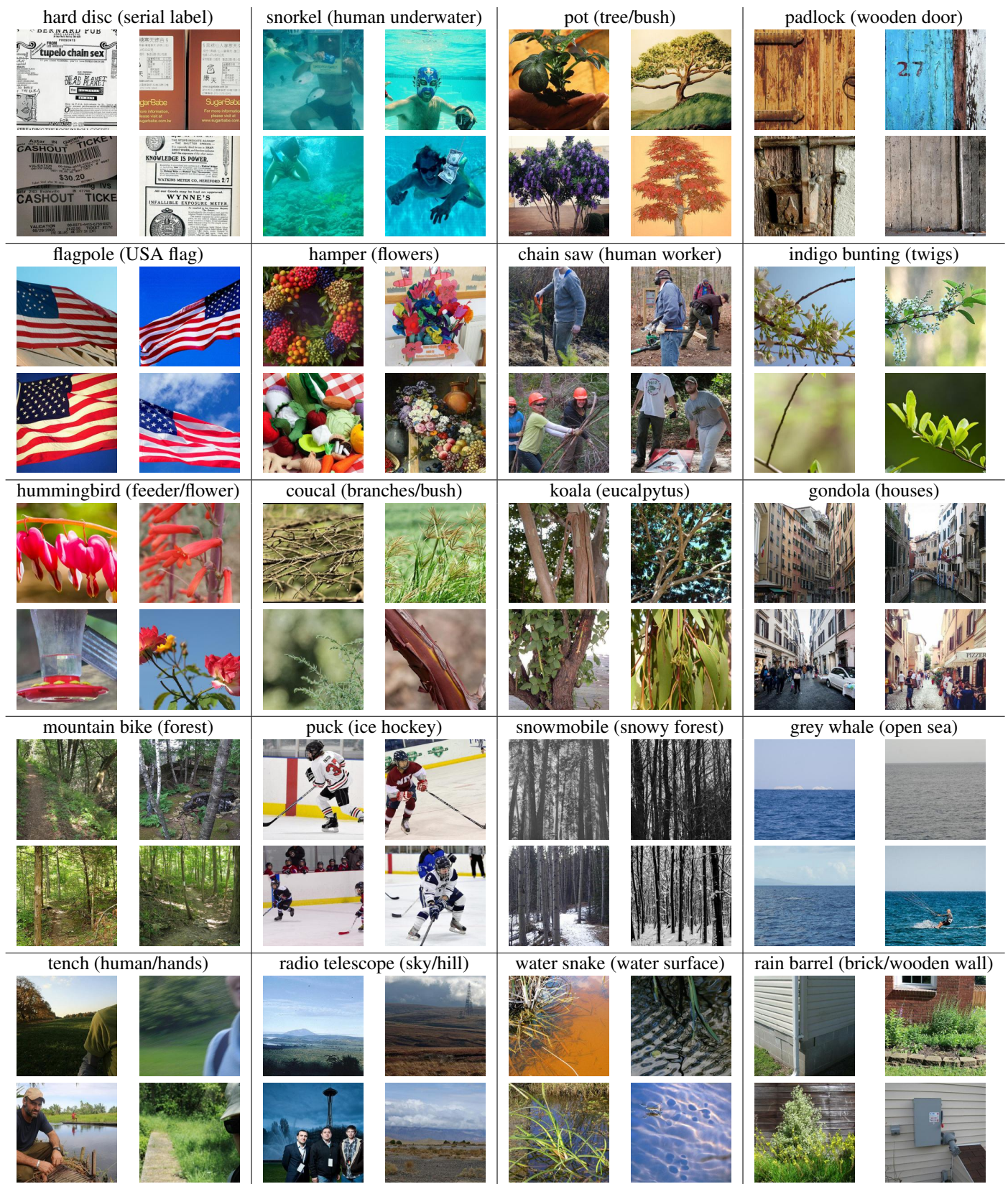


Figure 11. Random selection of 4 images for classes 1-20 of our “Spurious ImageNet” dataset with class label (spurious feature).

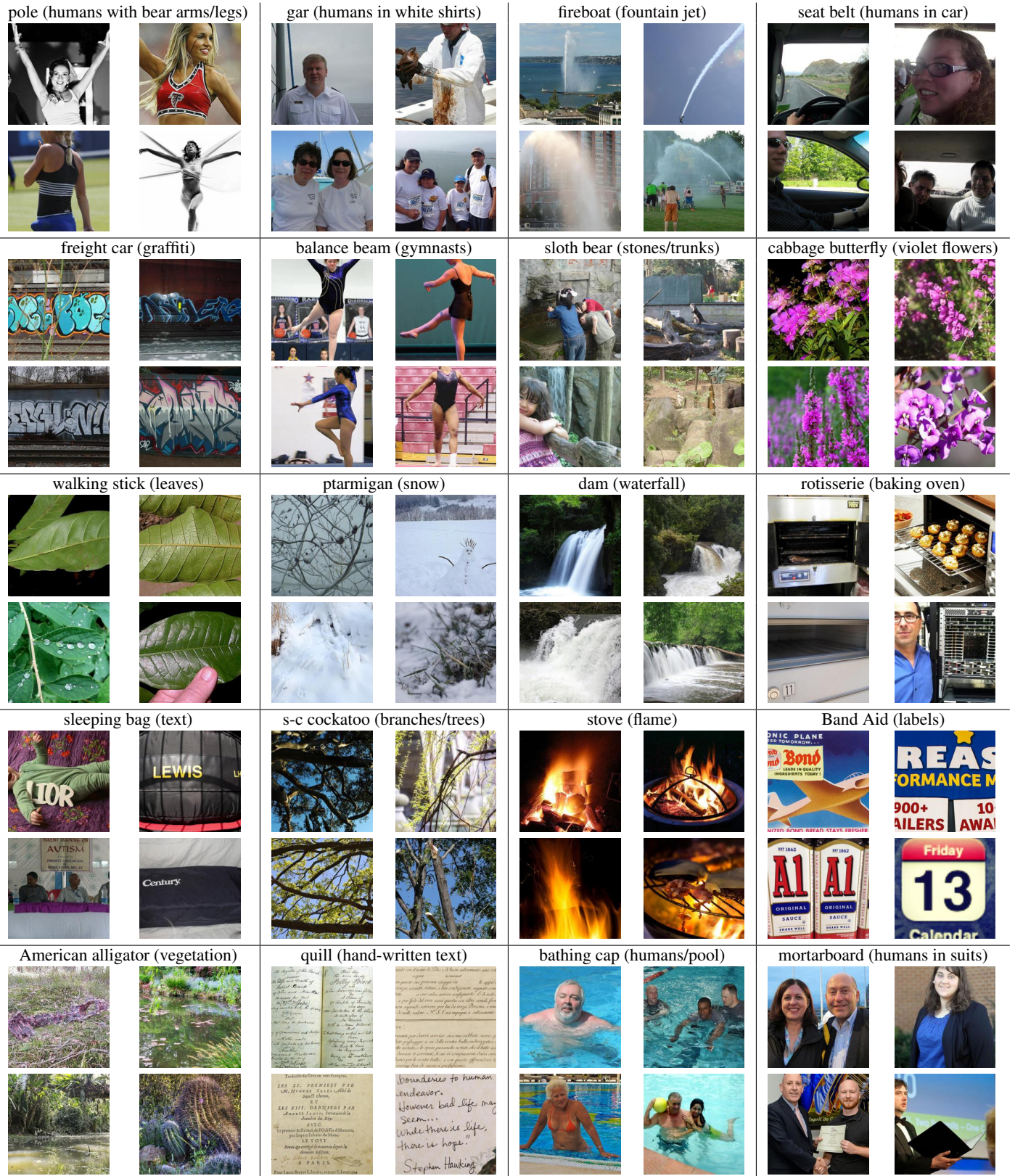


Figure 12. Random selection of 4 images for classes 21-40 of our “Spurious ImageNet” dataset with class label (spurious feature).

in1k			in1kFT21k			in21k	
Name	Acc. \uparrow	mAUC \uparrow	Name	Acc. \uparrow	mAUC \uparrow	Name	mAUC \uparrow
Rob. ResNet50	57.4	0.63	ResNetv2 152 BiT	84.9	0.87	ResNetv2 152 BiT	0.90
Rob. ResNet50 [45]	57.9	0.65	ResNetv2 50 BiT	84.0	0.88	ResNetv2 50 BiT	0.90
Rob. ResNet50 (SpuFix.)	56.8	0.78	EfficientNetv2 M	85.6	0.89	EfficientNetv2 M	0.92
ResNet50	80.4	0.83	EfficientNetv2 L	86.3	0.89	EfficientNetv2 L	0.93
ResNet101	81.9	0.76	ConvNeXt-B	85.8	0.87	ConvNeXt-L	0.94
ResNeXt50 32x4d	81.1	0.79	ConvNeXt-L	86.6	0.90	ConvNeXt-XL	0.95
ResNeXt101 32x8d	79.3	0.80	ConvNeXt-XL (384)	87.5	0.90	Swin-B p4 (224)	0.83
ResNeXt101 64x4d	83.1	0.77	DeiT3-S p16 (224)	83.1	0.83	Swin-L p4 (384)	0.84
EfficientNet B5	83.8	0.84	DeiT3-L p16 (384)	87.7	0.87	ViT-B p16 (224)	0.92
EfficientNet B5 AP	84.3	0.83	Swin-B p4 (224)	85.2	0.86	ViT-L p16 (224)	0.93
EfficientNet B6	84.1	0.83	Swin-L p4 (384)	87.2	0.89	BeiT-B p16 (224)	0.93
EfficientNet B6 AP	84.8	0.84	ViT-B p16 (224)	84.5	0.90	BeiT-L p16 (224)	0.93
EfficientNet B7	84.9	0.83	ViT-B p16 (384)	86.0	0.91		
EfficientNet B7 AP	85.1	0.82	ViT-L p16 (384)	87.1	0.93		
EfficientNetv2 M	85.0	0.84	ViT-L p16 (224)	85.8	0.92		
EfficientNetv2 L	85.5	0.85	BeiT-B p16 (224)	85.2	0.87		
ConvNeXt-B	83.8	0.79	BeiT-L p16 (512)	88.6	0.90		
ConvNeXt-L	84.3	0.79					
DeiT3-S p16 (224)	81.4	0.86					
DeiT3-L p16 (384)	85.8	0.86					
VOLO D5 (512)	87.0	0.87					
VOLO D3 (224)	85.4	0.85					

Table 2. Extended version of Tab. 1 from the main paper. We show ImageNet1k Accuracy and mean spurious AUC (mAUC) for a wide selection of state-of-the-art ImageNet models, trained on either ImageNet1k only (in1k), pre-trained on ImageNet21k and then fine-tuned on ImageNet1k (in1kFT21k) and full ImageNet21k classifiers (in21k). For models commonly used with different input resolutions, we state the used one in brackets.

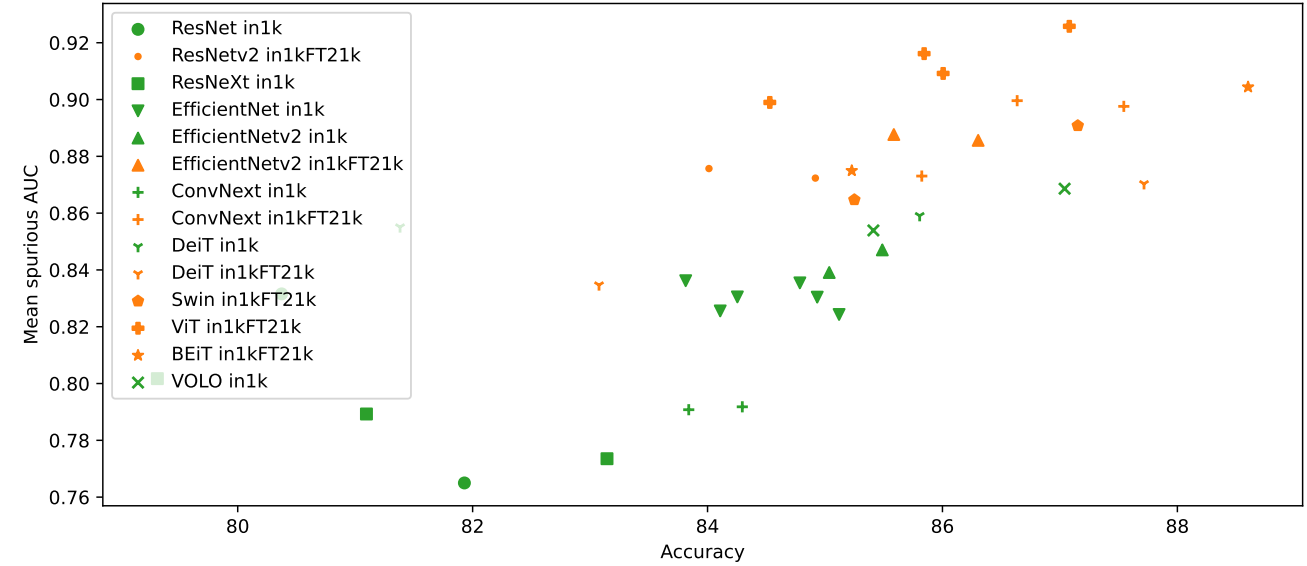


Figure 13. We plot Accuracy versus mean spurious AUC for a wide variety of SOTA ImageNet classifiers. All models that are pre-trained on ImageNet21k and then fine-tuned are marked in yellow whereas standard ImageNet1k models are marked green. As can be observed, pre-training on ImageNet21k does decrease vulnerability to spurious features over ImageNet1k models with comparable accuracy.

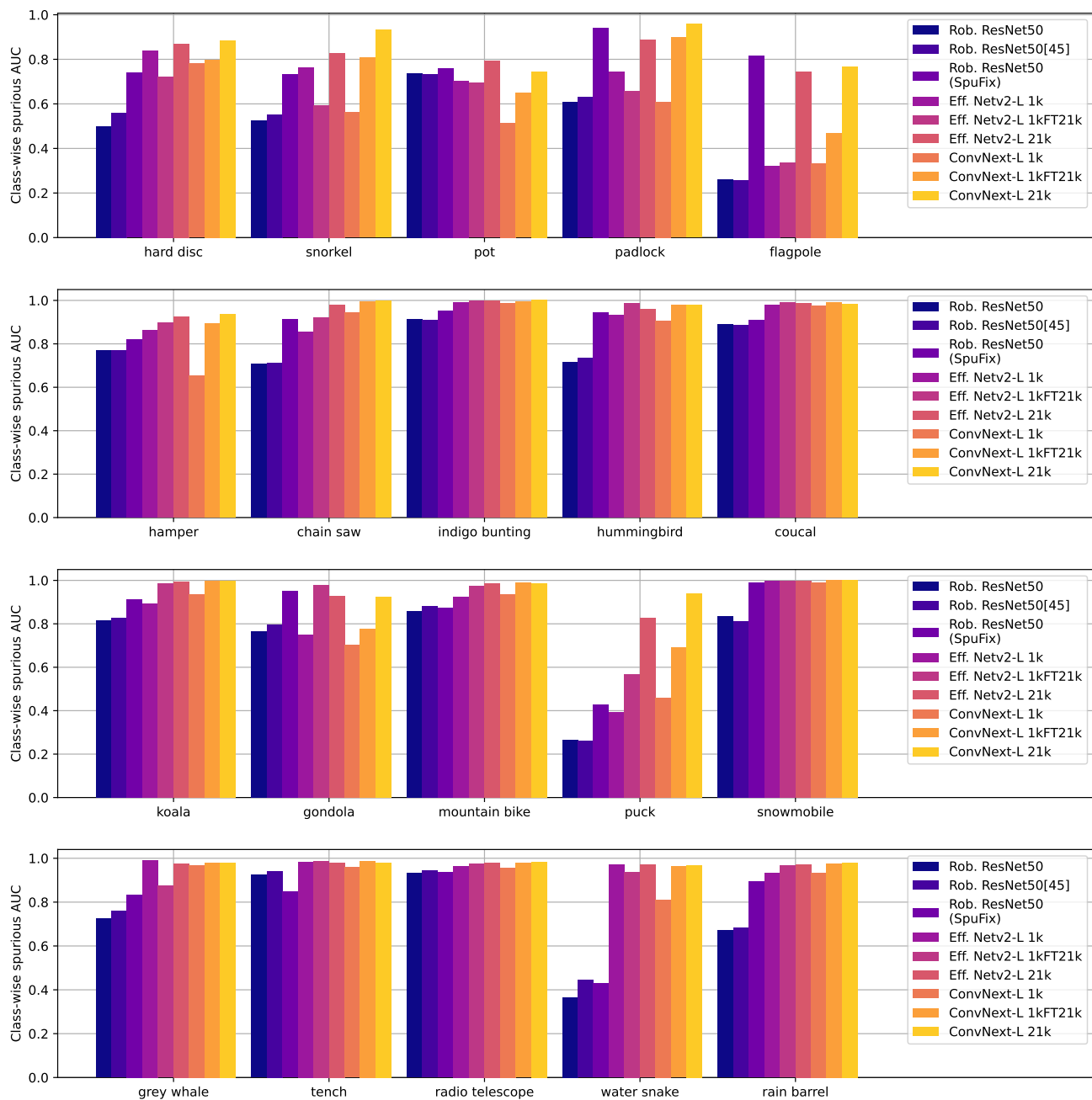


Figure 14. Extended version of Fig. 5 from the main paper for all 40 classes in our dataset. We plot class-wise spurious AUC for our robust ResNet50, the robust ResNet50 from [45], our robust ResNet50 with SpuFix as well as and EfficientNetv2-L and a ConvNext-L, both trained on ImageNet1k with and without pre-training on ImageNet21k as well as pure ImageNet21k training.

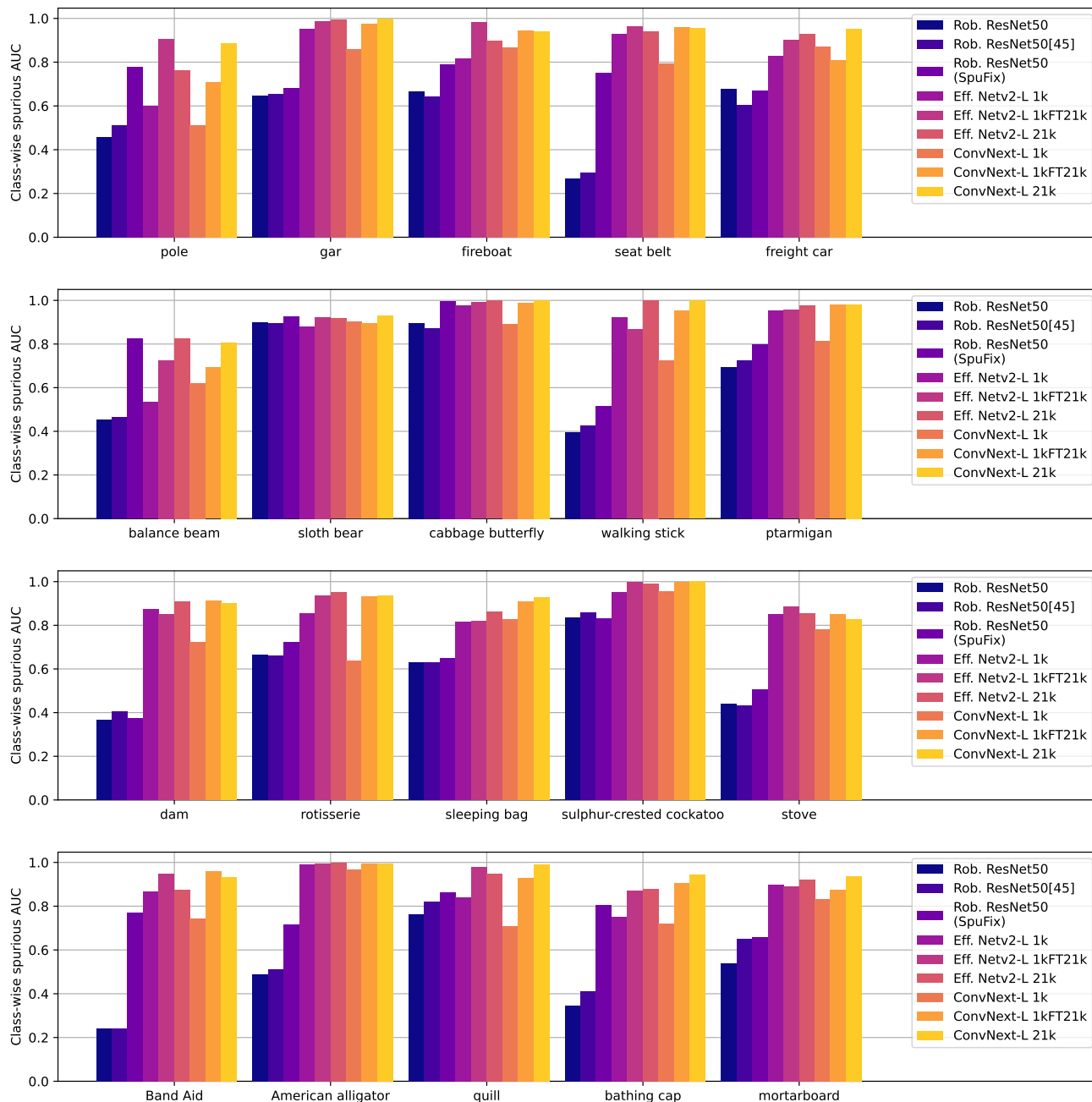


Figure 15. Continued from Fig. 14 for the remaining 20 classes.



Figure 16. We show all images of class “quill” (spurious feature: handwritten text) in Spurious ImageNet together with the top-3 predicted probabilities of the ConvNext-L-1kFT21k. Despite a class-wise AUC of 0.929 which seemingly suggests that the spurious feature is not playing a big role anymore, we observe that 76% of the images are classified as “quill” despite no “quill” being present. Thus the spurious class extension is still existing. The classifier just produces slightly less confident predictions on these images.






















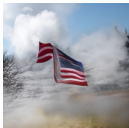














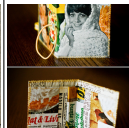
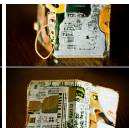
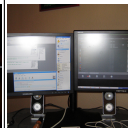

Original	DVCE	Original	DVCE	Original	DVCE	Original	DVCE	Original	DVCE
fountain: 0.36	fireboat: 0.53	fountain: 0.99	fireboat: 0.86	fountain: 0.82	fireboat: 0.98	fountain: 0.92	fireboat: 0.98	seashore: 0.42	fireboat: 1.0
									
stone wall: 0.93	freight car: 0.84	stone wall: 0.92	freight car: 1.0	stone wall: 0.93	freight car: 0.95	moving van: 0.17	freight car: 0.99	shopping cart: 0.95	freight car: 1.0
									
geyser: 0.99	flagpole: 1.0	alp: 0.33	flagpole: 1.00	mosque: 0.19	flagpole: 1.0	paddle: 0.14	flagpole: 0.99	stone wall: 0.21	flagpole: 1.0
									
car mirror: 1.0	hard disc: 0.92	gas pump: 0.42	hard disc: 0.99	stone wall: 0.93	hard disc: 0.93	comic book: 0.43	hard disc: 1.0	monitor: 0.57	hard disc: 0.97
									

Figure 17. Adding spurious features automatically with an adaptation of DVCEs [5] changes the prediction of the classifier Rob. ResNet50. This happens, because, as has been shown qualitatively in Fig. 4 and quantitatively in Fig. 5, this classifier has learned to associate class “fireboat” with the spurious feature “water jet”, “freight car” - with “graffiti”, “flagpole” with a flag without the pole and mostly with “US flag”, and “hard disc” - with “label”. This again confirms that they are *harmful* spurious features.